Large-momentum-transfer production of direct photons, jets, and particles

J. F. Owens

Department of Physics, Florida State University, Tallahassee, Florida 32306

The theoretical framework for describing the production of direct photons in hadronic collisions is reviewed. A detailed comparison between the theoretical predictions and existing data is presented along with a critical evaluation of the various sources of theoretical uncertainty. The information available from direct-photon experiments is contrasted with that learned from jet or single-hadron production. Prospects for new types of measurements in future experiments are also presented.

CONTENTS

I. INTRODUCTION

Over the last decade, quantum chromodynamics (QCD; Fritzsch, Gell-Mann, and Leutwyler, 1973) has emerged as a viable theory of the strong interaction. In this theory the interactions of hadrons are described in terms of the interactions among the hadronic constituents—quarks and gluons (occasionally referred to collectively as partons). One of the key features of the theory that has set it apart from earlier field-theoretic descriptions of strong-interaction dynamics is the property of asymptotic freedom (Gross and Wilczek, 1973a; Politzer, 1973). This term is used to describe the weakening of the effective quark-gluon coupling at short distances or, equivalently, large momentum transfers. The feature of asymptotic freedom allows the application of well-known perturbative techniques to the problem of obtaining predictions for processes that are dominated by short-distance interactions. It is for this reason that large-momentum-transfer processes have played an important role in the program of testing QCD.

It is a fortunate fact that the characteristic scale Λ for the momentum-transfer dependence of the effective or "running" coupling α_s is on the order of several hundred MeV. One consequence is that there are kinematic regions that can be readily accessed where α_s is sufficiently small to allow the use of perturbation theory. A comprehensive review of the various methods used to determine α_s has been provided by Duke and Roberts (1984), who include a thorough discussion of the experimental results.

The experiments that have been the easiest to interpret, and that, therefore, have provided the cleanest tests of the theory, all involve at least one electromagnetic vertex. Examples include e^+e^- annihilation, deep-inelastic scattering of leptons from nucleons, and high-mass lepton pair production in hadronic collisions. The pointlike nature of the quark-photon vertex allows for the control of the reaction kinematics at the level of the parton interactions. With a definite theory for the short-distance phenomena, such processes can be used to study the substructure of the initial-state hadrons and the manner in which the scattered constituents give rise to the final-state hadrons. However, it is also important to verify the description of the short-distance interactions and, therefore, it is necessary to consider processes in which the constituents of one hadron can undergo hard scatters with those of another hadron. The production of hadrons with large transverse momentum in hadron-hadron interactions can provide such information. These reactions have been studied extensively, and a consistent description of the data can be obtained using QCD. Recently the production of large-transverse-momentum hadronic jets, especially at the very high energies available at the CERN $Sp\bar{p}S$ Collider, has emerged as another area in which QCD is able to provide a good description of the data. Here the term "jet" refers to a collimated collection of hadrons emerging from a hard-scattering reaction. Jets result from the process of hadronization, wherein the scattered partons are converted to the hadrons appearing in the final state. The four-vector of the jet is closely related to that of the parent parton, so that by studying jet production one can get closer to the underlying parton-level kinematics.

Hadron-hadron processes are rather complicated at the level of the constituent quarks and gluons. Many subprocesses have to be summed over, and, for example, in the calculation of the invariant cross section for single-

particle inclusive hadron production using three quark flavors, there are 127 separate two-body scattering contributions. Furthermore, one really is interested in studying the interactions of the constituents, and the final-state hadrons provide, at best, an indirect probe. Jets are, in principle, better in this regard, but there are ambiguities related to the algorithm used to identify the jets experimentally, and one still has the same number of subprocesses to disentangle. It is, therefore, of interest to consider a large-momentum-transfer hadron-hadron scattering process in which one can directly constrain the underlying kinematics of a small number of subprocesses. Such a reaction is direct-photon production. Here the term "direct photon" is taken to mean a photon that originates from an interaction related to the hard scatter and not from the production of a hadron that subsequently decays electromagnetically. Since the direct photon originates in the hard-scattering subprocess, one has a more direct probe of the interaction. Furthermore, the photon couples to electric charge, while the quarks and gluons interact via the color charges. Thus direct-photon production yields information that is complementary to that obtained from hadron and jet production.

Although the above argument in favor of measuring direct-photon production may seem reasonable, one must still worry about the question of rate. At first glance, one might expect that the γ/hadron ratio would be of order α. Actually, however, it is the γ/jet cross-section ratio that is of order α. This is easily understood since the dominant subprocesses for direct-photon production are similar to those for jet production, except that a gluon is replaced by a photon. Furthermore, it is experimentally known that the jet/hadron ratio varies between 10^2 and 10^3 depending on the kinematic region of interest. Therefore the photon/hadron ratio might well be of order 1 or larger. In reality there are more subprocesses for jet production, so that this is somewhat of an overestimate. Nevertheless, experiments have already shown that the γ/π ratio is sizable and approaches one at the highest p_T values for which data are available. These data have established that the direct-photon signal can be measured in the high-p_T region, therefore opening the way for more detailed measurements of the process.

A process closely related to direct-photon production is that of lepton pair production. This, too, is basically an electromagnetic probe of the hard-scattering process. This process is somewhat more complicated due to the presence of another kinematic variable—the dilepton invariant mass. The production of massive lepton pairs at large transverse momentum provides a classic example of a problem with two large scales. Although more complicated than processes with a single large scale, a formalism for this problem has been developed (Altarelli, Ellis, Greco, and Martinelli, 1984; Collins, Soper, and Sterman, 1985).

Recently a review by Ferbel and Molzon (1984) of the experimental status of direct-photon production was published. There a summary of existing experimental results was presented along with a comparison with various theoretical calculations. In addition, a discussion of "second-generation" experiments was presented. The purpose of this paper is to provide a detailed description of the theoretical calculations that have been performed for direct-photon production. In this sense, this work is intended as a complementary review that can be used in conjunction with the work of Ferbel and Molzon. Furthermore, new data have recently become available for direct-photon and jet production. The increased coverage in p_T and center-of-mass energy have made it possible to present a more detailed phenomenological analysis than was previously possible. New theoretical work in the area of next-to-leading-logarithm calculations has also been completed in the last year. The results will be reviewed in some detail, and their impact on future theoretical analyses of data will be discussed.

In the next section the basic theoretical formalism will be reviewed. Particular attention will be paid to sources of theoretical uncertainty and how this may be reduced in the future. Section III contains a comparison between the theoretical predictions and existing data. Since the maximum amount of information can be extracted from direct-photon production only when it is compared with other high-p_T processes, a brief comparison with data on jet and single-hadron production is also included. This will serve as a check on such things as the choice of distribution and fragmentation functions, factorization scale, etc. The goal is to see whether or not a consistent description of hadron, jet, and photon production can be obtained. In this context the role of calculations of next-to-leading logarithm contributions will be discussed. Section III also contains a discussion of types of measurements that can be performed using the forthcoming second-generation detectors. These include measurements of parton-parton scattering angular distributions, the extraction of information on gluon distributions, and more detailed hadron-photon correlation measurements. Section IV contains a final discussion and summary. In order to preserve continuity in the text, an Appendix has been provided that contains details concerning the notation, kinematics, and the calculation of the observables discussed in the review.

II. FORMALISM

A. Cross sections and other observables

The application of QCD to various hard-scattering processes has been reviewed frequently. Some useful references for general applications include those of Field, 1978; Ellis and Sachrajda, 1979; Reya, 1981; Owens, 1982b; and Pennington, 1983. The specific results needed for describing high-p_T hadronic interactions have also been reviewed in the past. Rather than repeat the basic background material in detail, I shall assume some familiarity with the hard-scattering formalism. Reviews that may be of use in understanding the formalism and past interpretations of the data include those of Sivers, Brod-

sky, and Blankenbecler, 1976; Ellis and Stroynowski, 1977; Jacob and Landshoff, 1978; McCubbin, 1981; Owens, 1982a; and Møller, 1984.

As an aid to someone who is unfamiliar with the kinematics and notation used in describing high-p_T phenomena, a brief summary is contained in the Appendix. Included there as well is a brief summary of the expressions for the observables discussed in this review.

The use of perturbation theory in QCD calculations is made possible by the feature of asymptotic freedom. If a process involves a large momentum transfer, then the running coupling α_s (to be discussed in detail below) may be small enough to justify the use of perturbative techniques. Thus, for example, one can calculate perturbatively the hard scattering of the hadron constituents in high-p_T processes. However, we deal experimentally with beams and targets consisting of hadrons, not partons. The calculation of the momentum distributions of partons inside hadrons requires knowledge of hadron wave functions in regions in which perturbation theory cannot be applied and we do not, as yet, have the ability to calculate such wave functions nonperturbatively. Accordingly, one must find a method to bridge the gap between what can be measured experimentally and what can be calculated perturbatively.

The prescription provided by the parton model has met with much success in describing a variety of large-momentum-transfer processes. Here it is assumed that one can factorize the process into two parts by utilizing the impulse approximation. The probability of finding a parton a in a hadron A with a momentum fraction lying between x and $x + dx$ is denoted by the distribution function $G_{a/A}(x)$. The probability of obtaining a hadron C with a momentum fraction between z and $z + dz$ from a parton c is denoted by the fragmentation function $D_{C/c}(z)$. These functions cannot be calculated using per-
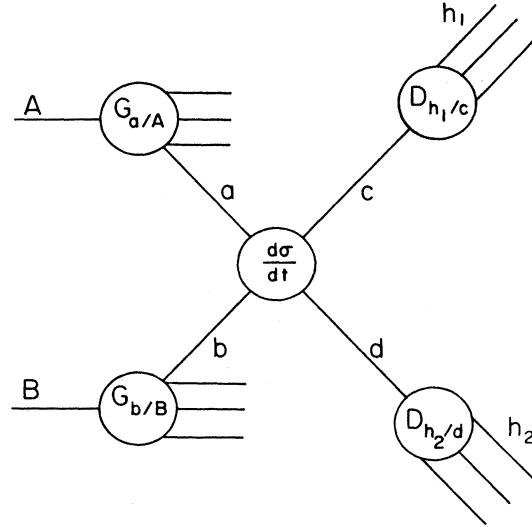

FIG. 1. Schematic representation of a high-p_T reaction factorized into parton distribution functions (G), parton fragmentation functions (D), and a hard-scattering subprocess.

turbation theory and must, therefore, be obtained from data for various types of hard-scattering processes. The cross section for the process under consideration is then built up by an incoherent summation over all possible constituent scatterings, each of which is weighted by the appropriate parton distribution and fragmentation functions. In the parton model the hard scattering is described by the lowest-order subprocesses which, for high-p_T particle, jet, or photon production, correspond to two-body scattering. This is shown schematically in Fig. 1. The corresponding expression for the invariant cross section is

$$E_C \frac{d\sigma}{d^3 p_C}(AB \rightarrow C + X) = \sum_{abcd} \int dx_a dx_b dz_c \, G_{a/A}(x_a) G_{b/B}(x_b) D_{C/c}(z_c) \frac{\hat{s}}{z_c^2 \pi} \frac{d\sigma}{d\hat{t}}(ab \rightarrow cd) \delta(\hat{s} + \hat{t} + \hat{u}) . \tag{1}$$

The δ function appearing in Eq. (1) is appropriate for the two-body scattering of massless partons and follows simply from two-body phase space. Furthermore, the initial and final partons have been assumed to be collinear with the corresponding initial and final hadrons, i.e., no parton transverse-momentum (k_T) smearing has been included. The effects resulting from the inclusion of nonzero parton k_T's will be discussed later.

The parton distribution and fragmentation functions must be determined by measurements made using some reference process. For example, the distribution functions are often determined by measurements made in deep-inelastic lepton-nucleon scattering, and fragmentation functions are often studied in $e^+ e^-$ annihilation or deep-inelastic scattering. In these processes the virtual photon or weak boson serves as a probe of the distribution

being studied, and the invariant mass squared of the virtual boson can be taken as an indicator of the length scale that is being probed. In this sense a large virtual mass corresponds to a short distance and vice versa. In the parton model these distributions do not depend on the value of the virtual mass and, therefore, are said to be scale invariant.

The prescription corresponding to Fig. 1 and Eq. (1) corresponds to retaining only the lowest-order scattering subprocesses which, in this case, corresponds to just two-body scattering. In QCD perturbation theory one must, of course, consider the contributions from more complicated scatterings. When higher-order subprocesses are considered, one encounters a variety of singularities that must be treated with care in order to obtain finite results. For example, consider the Feynman graphs shown in Fig.

2. Those in Fig. 2(a) are for the QCD Compton subprocess $gq \rightarrow \gamma q$, while those in Fig. 2(b) are for the annihilation subprocess $q\bar{q} \rightarrow \gamma g$. Figures 2(c)–2(e) represent some of the various $O(\alpha\alpha_s^2)$ subprocesses that contribute to direct-photon production. The eight graphs in Fig. 2(c) arise from allowing an additional gluon to be present in the final state of Compton process in Fig. 2(a). Consider the first graph in Fig. 2(c), in which a gluon is radiated from the incoming quark leg of the Compton subprocess. If the initial quark and the emitted gluon become collinear, then the internal quark line to which they are connected will become "on-shell," i.e., the invariant mass corresponding to the internal quark line will become zero. In QED such a configuration would contribute to the radiative corrections for the particular process, and there would be a logarithmic correction proportional to $\ln s/m_{\text{lepton}}^2$, where s is the square of the center-of-mass energy. In QCD, however, the partons are treated as massless and the logarithm becomes infinite. This class of singularities is referred to, appropriately, as mass singularities. These logarithmically divergent terms would appear to ruin the calculation. However, it can be
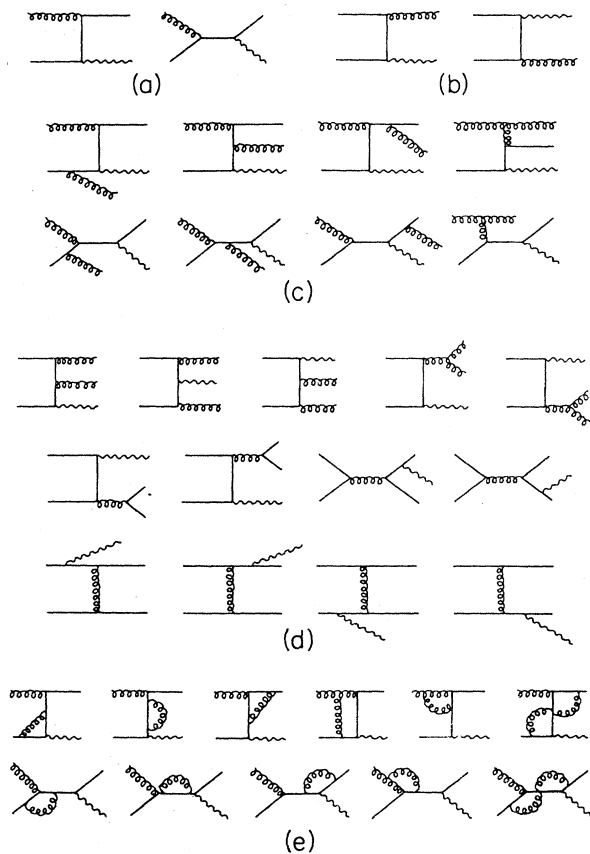

(a)   (b)

(c)

(d)

(e)

FIG. 2. Selection of Feynman diagrams for direct-photon production: (a) $O(\alpha\alpha_s)$ Compton subprocess; (b) $O(\alpha\alpha_s)$ annihilation subprocess; (c) $O(\alpha\alpha_s^2)$ subprocess $gq \rightarrow \gamma qg$; (d) $O(\alpha\alpha_s^2)$ subprocess $q\bar{q} \rightarrow \gamma gg$; (e) one-loop graphs for the Compton subprocess that contribute to the $O(\alpha\alpha_s^2)$ calculation.

shown that these singularities are universal in the sense that they appear in the same way in all subprocesses containing a given species of parton. It can also be shown that the singularities can be factorized or separated from the relevant subprocesses (Ellis, Georgi, Machacek, Politzer, and Ross, 1978, 1979; Gupta and Mueller, 1979). The use of this factorization theorem allows one to separate out the mass singularities and absorb them into the uncalculated portions of the distribution and fragmentation functions. These are, in turn, specified through the use of some reference process such as deep-inelastic lepton-nucleon scattering or e^+e^- annihilation. In a sense, then, the problem of the mass singularities is sidestepped by using reference processes to define the various parton distribution and fragmentation functions. These finite quantities are then used in the calculation of other hard-scattering reactions.

In addition to the mass singularities there are ultraviolet singularities associated with the loops appearing in the graphs of Fig. 2(e). These must be regulated by some technique (such as dimensional regularization) and then subtracted. These two steps constitute the process of renormalization. Finally, the remaining infrared or soft singularities will cancel when the results for all of the loop graphs [such as Fig. 2(e)] and the tree graphs [such as Fig. 2(c)] are added together. It would be beyond the scope of this review to give the details of the above procedures whereby the higher-order corrections are rendered finite. However, this has been discussed in great detail by Buras (1980), for example.

One way of viewing the factorization procedure is to think of partitioning a given process in the manner indicated in Fig. 1. There is a hard scattering that takes place between the interacting partons and that can be calculated perturbatively. The distribution and fragmentation functions relate the partons to the external hadrons. So far, this is just the usual parton model picture. Now, however, certain elements of the parton scattering processes can be thought of as being radiative corrections to the incoming and outgoing partons. These radiative corrections give rise to momentum-dependent distribution and fragmentation functions. The original scale-invariant distributions have now been modified, and the changes with momentum transfer are referred to as scaling violations.

In order to implement the factorization discussed above, it is necessary first to specify a momentum scale at which the procedure is to take place. The term "scale" is, perhaps, somewhat overused. However, the terminology is often encountered in the literature and I shall continue to use it here. In the present context "scale" can be thought of as being synonymous with variable. The factorization scale, denoted by M^2, is defined in terms of the kinematic variables that describe the process under consideration. The net result is to introduce a logarithmic M^2 dependence into the distribution and fragmentation functions coming from the radiative corrections mentioned above. This logarithmic behavior is, in fact, the remnant of the mass singularities that have been factorized off. If one works to all orders of perturbation theory

and retains the leading logarithmic contribution from each order, then this is the so-called leading-logarithm approximation. The final answer, then, in this approximation, consists of M^2 dependent distribution and fragmentation functions convoluted with the lowest-order parton scattering subprocesses. It is also possible to include systematically the next-to-leading-logarithm contributions, as will be discussed later in this section.

An additional modification to Eq. (1) must be made when the effects of higher-order terms are incorporated. It is possible to take into account certain vertex and gluon propagator corrections by replacing the strong coupling constant with one that depends on a momentum scale characteristic of the process considered. This scale-dependent, or running, coupling α_s is introduced in the process of solving the renormalization group equation. When the process of renormalization is implemented, it is necessary to specify a point at which the coupling of the theory will be defined. This renormalization point will be denoted by a momentum transfer μ. Now, different choices of μ will result in different values for the coupling α_s. Since α_s is dimensionless, the dependence on the renormalization point in regions of large momentum transfers Q^2 must be through dimensionless ratios of the form Q^2/μ^2. The dependence of α_s on Q^2 is given by

$$\frac{d\alpha_s(t)}{dt}=\beta[\alpha_s(t)] , \qquad (2)$$

where $t=\ln(Q^2/\mu^2)$ and the function β determines the change in the coupling as the renormalization point μ is changed. β can be calculated for QCD using perturbation theory (Gross and Wilczek, 1973a; Politzer, 1973), with the result that to two-loop order

$$\beta(\alpha_s)=-b\alpha_s^2-c\alpha_s^3 ,$$

where

$$b=\frac{33-2f}{12\pi} \text{ and } c=\frac{153-19f}{24\pi^2}$$

with f denoting the number of quark flavors. If Eq. (2) is integrated using the one-loop approximation for β ($c=0$), one finds

$$\alpha_s(t)=\frac{\alpha_s(0)}{1+\alpha_s(0)bt} .$$

The explicit dependence on $\alpha_s(0)$ can be removed by defining a scale parameter Λ by

$$\Lambda^2=\mu^2 e^{-1/\alpha_s(0)b} ,$$

so that

$$\alpha_s(Q^2)=\frac{12\pi}{(33-2f)\ln(Q^2/\Lambda^2)} . \qquad (3)$$

The large momentum variable Q^2 need not necessarily be the same as the factorization scale M^2. The constant Λ appearing in Eq. (3) sets the scale for the Q^2 dependence and will be discussed in more detail in connection with the next-to-leading-order corrections.

In the leading-logarithm approximation the modified form of Eq. (1) is now

$$E_C=\frac{d\sigma}{d^3p_C}(AB\rightarrow C+X)=\sum_{abcd}\int dx_a dx_b dz_c G_{a/A}(x_a,M_d^2)G_{b/B}(x_b,M_d^2)D_{C/c}(z_c,M_f^2)\frac{\hat{s}}{z_c^2\pi}\frac{d\sigma}{d\hat{t}}(ab\rightarrow cd)\delta(\hat{s}+\hat{t}+\hat{u}) , \qquad (4)$$

with the subprocesses calculated using the strong running coupling of Eq. (3). For the case of hadron or jet production the relevant subprocesses include all possible two-body quark-quark, quark-gluon, and gluon-gluon scatterings. For the case of direct photons one must consider, as well, the subprocesses $qg\rightarrow q\gamma$ and $q\bar{q}\rightarrow g\gamma$. The expressions for these subprocesses are summarized in Table I.

Notice in Eq. (4) that allowance has been made for different factorization scales for the fragmentation and distribution functions. There are thus three different scales that must be chosen—Q^2, M_d^2, and M_f^2. The distinction among the various scales is relevant when one considers the next-to-leading-logarithm corrections. However, the distinction can, in principle, be ignored if one is working only in the leading-logarithm approximation, since then all large momentum scales are equivalent.

It is perhaps appropriate at this point to discuss briefly the limitations on the region of validity of Eq. (4). The leading-logarithm approximation relies on the presence of a single large momentum scale that characterizes the process under consideration. For high-p_T reactions, such a scale could be p_T^2, for example. The fact that there should be only a single large scale can be shown by the following simple argument. Suppose that one has two such scales—Q_1^2 and $Q_2^2=kQ_1^2$, where k is a constant. Then,

$$\ln Q_2^2=\ln(Q_1^2)[1+(\ln k)/(\ln Q_1^2)]$$

$$=\ln(Q_1^2)[1+\cdots]$$

$$\approx\ln(Q_1^2) ,$$

where the dots serve to indicate that the terms dropped contained nonleading logarithmic terms. Therefore all large scales are equivalent in the region where the leading-logarithm approximation is truly applicable. This region is where $\hat{s}\sim-\hat{t}\sim-\hat{u}$ and $\alpha_s(Q^2)$ is much less than one. In practice, these two constraints are often satisfied only in regions for which there are no data. Thus, when comparing predictions based on the leading-logarithm approximation with available data, it may well make a significant difference as to which choice is made for the large scale. Examples of this will be discussed further in Sec. III.

The formalism used in deriving Eq. (4) can also be used to generate predictions for other types of observables,

TABLE I. Expressions for the parton-parton two-body scattering differential cross sections. A factor of $\pi\alpha_s^2/s^2$ has been factored out of the purely strong-interaction processes. Factors of $\pi\alpha\alpha_s/s^2$ and $\pi\alpha^2/s^2$ have been factored out of the single- and double-photon subprocesses, respectively. e_q denotes the fractional charge of a quark. All of the Mandelstam variables refer to the parton level (the caret symbol used in the text has been deleted for clarity).

Subprocess	Cross section
$qq' \rightarrow qq'$	$\dfrac{4}{9}\dfrac{s^2+u^2}{t^2}$
$qq \rightarrow qq$	$\dfrac{4}{9}\left[\dfrac{s^2+u^2}{t^2}+\dfrac{s^2+t^2}{u^2}\right]-\dfrac{8}{27}\dfrac{s^2}{tu}$
$q\bar{q} \rightarrow q'\bar{q}'$	$\dfrac{4}{9}\dfrac{t^2+u^2}{s^2}$
$q\bar{q} \rightarrow q\bar{q}$	$\dfrac{4}{9}\left[\dfrac{s^2+u^2}{t^2}+\dfrac{u^2+t^2}{s^2}\right]-\dfrac{8}{27}\dfrac{u^2}{st}$
$gq \rightarrow gq$	$-\dfrac{4}{9}\left[\dfrac{s}{u}+\dfrac{u}{s}\right]+\dfrac{s^2+u^2}{t^2}$
$q\bar{q} \rightarrow gg$	$\dfrac{32}{27}\left[\dfrac{t}{u}+\dfrac{u}{t}\right]-\dfrac{8}{3}\dfrac{t^2+u^2}{s^2}$
$gg \rightarrow q\bar{q}$	$\dfrac{1}{6}\left[\dfrac{t}{u}+\dfrac{u}{t}\right]-\dfrac{3}{8}\dfrac{t^2+u^2}{s^2}$
$gg \rightarrow gg$	$\dfrac{9}{2}\left[3-\dfrac{tu}{s^2}-\dfrac{su}{t^2}-\dfrac{st}{u^2}\right]$
$gq \rightarrow \gamma q$	$-\dfrac{e_q^2}{3}\left[\dfrac{u}{s}+\dfrac{s}{u}\right]$
$q\bar{q} \rightarrow \gamma g$	$\dfrac{8}{9}e_q^2\left[\dfrac{u}{t}+\dfrac{t}{u}\right]$
$q\bar{q} \rightarrow \gamma\gamma$	$\dfrac{2}{3}e_q^4\left[\dfrac{t}{u}+\dfrac{u}{t}\right]$

$gg \rightarrow \gamma\gamma$

$$\left[\sum_{i=1}^{n_f}e_q^2\right]^2\frac{\alpha_s^2}{8\pi^2}\left\{\frac{1}{8}\left\{\left[\frac{s^2+t^2}{u^2}\ln^2\left(-\frac{s}{t}\right)+2\frac{s-t}{u}\ln\left(-\frac{s}{t}\right)\right]^2\right.\right.$$

$$\left.+\left[\frac{s^2+u^2}{t^2}\ln^2\left(-\frac{s}{u}\right)+2\frac{s-u}{t}\ln\left(-\frac{s}{u}\right)\right]^2+\left[\frac{t^2+u^2}{s^2}\left(\ln^2\frac{t}{u}+\pi^2\right)+2\frac{t-u}{s}\ln\frac{t}{u}\right]^2\right\}$$

$$\times\frac{1}{2}\left[\frac{s^2+t^2}{u^2}\ln^2\left(-\frac{s}{t}\right)+2\frac{s-t}{u}\ln\left(-\frac{s}{t}\right)+\frac{s^2+u^2}{t^2}\ln^2\left(-\frac{s}{u}\right)+2\frac{s-u}{t}\ln\left(-\frac{s}{u}\right)\right.$$

$$\left.+\frac{t^2+u^2}{s^2}\left(\ln^2\frac{t}{u}+\pi^2\right)+2\frac{t-u}{s}\ln\frac{t}{u}\right]$$

$$\left.+\frac{\pi^2}{2}\left\{\left[\frac{s^2+t^2}{u^2}\ln\left(-\frac{s}{t}\right)+\frac{s-t}{u}\right]^2+\left[\frac{s^2+u^2}{t^2}\ln\left(-\frac{s}{u}\right)+\frac{s-u}{t}\right]^2\right\}+4\right]$$

such as correlations between a high-p_T trigger hadron or photon and additional hadrons or photons in the event. Such correlations will be discussed in Sec. III in detail. The required expressions are collected in the Appendix.

B. Distribution and fragmentation functions

In order to use Eq. (4) one must have available the relevant distribution and fragmentation functions at the appropriate factorization scales. These are typically ob-

tained by first fitting some parametrization to data from deep-inelastic scattering or e^+e^- annihilation at a scale Q_0^2. The evolution from Q_0^2 to some other scale Q^2 can then be calculated using the Altarelli-Parisi equations (Altarelli and Parisi, 1977) for the distribution functions or their equivalent for the fragmentation functions (Owens, 1978; Uematsu, 1978). These are a set of coupled differential-integral equations that describe the Q^2 dependence of the quark and gluon distribution or fragmentation functions. For the case of the distribution functions, they are

$$\frac{dG_{q_i/A}(x,Q^2)}{dt} = \frac{\alpha_s(Q^2)}{2\pi} \int_x^1 \frac{dy}{y} [P_{qq}(x/y)G_{q_i/A}(y,Q^2) + P_{qg}(x/y)G_{g/A}(y,Q^2)]$$ (5a)

and

$$\frac{dG_{g/A}(x,Q^2)}{dt} = \frac{\alpha_s(Q^2)}{2\pi} \int_x^1 \frac{dy}{y} \left[\sum_i P_{gq}(x/y)G_{q_i/A}(y,Q^2) + P_{gg}(x/y)G_{g/A}(y,Q^2) \right].$$ (5b)

Here t is defined as $\ln(Q^2/\Lambda^2)$. The splitting functions P_{ij} can be found in Altarelli and Parisi, (1977), for example, and are simply the inverse Mellin transforms of the appropriate anomalous dimensions specified by the theory (Gross and Wilczek, 1973b).

Recently an analysis of data from deep-inelastic scattering, J/ψ, Υ, and high-mass dilepton production was performed in order to determine a set of nucleon-parton distributions (Duke and Owens, 1984). If one uses only deep-inelastic scattering data, there is not a great deal of sensitivity to the gluon distribution function. There is, instead, a strong correlation between the shape of the gluon distribution and the value of Λ obtained in the fitting process (Barnett and Schlatter, 1982; Devoto, Duke, Owens, and Roberts, 1983). A harder (i.e., flatter) gluon distribution results in a larger value of Λ and vice versa. In addition, with the data sets currently available, the precise choice of W^2 and Q^2 cuts, the Fermi motion corrections, the parametrization choice, and the fitted x range can strongly influence the final results (Devoto, Duke, Owens, and Roberts, 1983). For these reasons it was decided to use data from J/ψ, Υ, and dilepton production in the analysis, in an attempt to obtain more constraints on the fitted distributions. The results, referred to as Set 1, yielded a relatively soft gluon distribution that behaves roughly as $(1-x)^5$ at $Q^2=10$ GeV^2 and a value for Λ of 200 MeV. Of course, it can be argued that nuclear effects might complicate the interpretation of those dilepton data obtained using nuclear targets, and that the use of the J/ψ and Υ data requires model-dependent assumptions. Accordingly, a fit only to the deep-inelastic data was performed, and the gluon distribution was constrained to be somewhat harder. This resulted in the Set 2 distributions with a value for Λ of 400 MeV. The input gluon distributions at $Q_0^2=4$ GeV^2 are shown for the two

sets in Fig. 3(a), while 3(b) shows a similar comparison at $Q^2=1000$ GeV^2. As the value of Q^2 is increased, the evolution drives the two gluon distributions closer together. The larger value of Λ associated with the harder gluon results in a faster evolution than for the softer gluon. Therefore at very large momentum transfers the
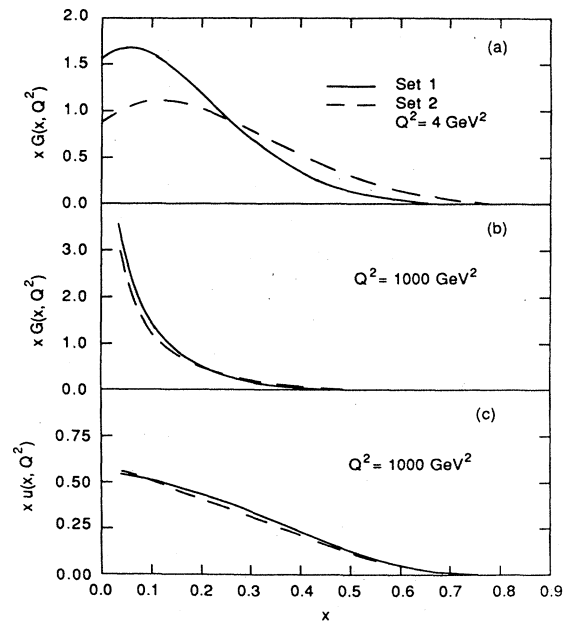

FIG. 3. Comparison of some of the Set 1 (solid curves) and Set 2 (dashed curves) parton distribution functions from Duke and Owens (1984): (a) gluon distributions at $Q^2=4$ GeV^2; (b) gluon distributions at $Q^2=1000$ GeV^2; (c) u-quark distributions at $Q^2=1000$ GeV^2. Each distribution has been multiplied by x.

differences between the predictions obtained with the two different sets of distribution functions tend to diminish. Specific examples of this effect will be shown in Sec. III. In Fig. 3(c) the u-quark distributions from both Sets 1 and 2 are compared at $Q^2 = 1000$ GeV^2. Again, very little difference can be observed between the two at this large value of Q^2. Convenient parametrizations of the two sets of nucleon distributions can be found in Duke and Owens (1984). That reference also compares the parametrizations with others that have appeared in the literature. Additional details of the analysis and the parametrizations may be found in the indicated reference.

High-p_T data are also available from pion beams. A companion analysis to that of Duke and Owens has been performed for pions (Owens, 1984), and parametrizations corresponding to Sets 1 and 2 nucleon distributions are contained therein. These two sets of pion and nucleon distributions will be used throughout the remainder of this review.

The fragmentation process, whereby the scattered partons generate the hadrons in the final state, has been studied extensively in a variety of reactions, with the bulk of our present information coming from e^+e^- annihilation studies. It is well known that if one wishes to describe accurately the distributions of all of the hadrons simultaneously, then the simple concept of fragmentation functions is not adequate. Instead, one needs to use more elaborate event generators based on string or cluster models. However, the generalization of such models to high-p_T hadron-hadron processes is a subject that is still under active investigation (Sjöstrand, 1985; Gottschalk, 1986). Fortunately, the types of observables that will be considered in this review do not require the simultaneous tracking of all the hadrons in a particular event. For single-particle cross sections and two-particle correlations, it often turns out that a simple set of fragmentation functions is sufficient, as will be shown shortly.

The fragmentation functions to be used in this review were obtained by first fitting data on hadron production from relatively low Q^2 deep-inelastic scattering and e^+e^- annihilation experiments. The fragmentation products include pseudoscalar and vector mesons as well as baryons. The Q^2 dependence was calculated using the appropriately modified evolution equations (Owens, 1978; Uematsu, 1978), and the vector mesons were then allowed to decay, with the appropriate decay branching ratios taken into account. This procedure is discussed in detail by Owens (1979), who also gives the specific input parametrizations used. After the Q^2 evolution and meson decay steps, the fragmentation functions depend on both the momentum fraction z and Q^2. The various distributions were stored in a set of two-dimensional arrays, and interpolation between the tabulated Q^2 and z points was used to obtain the functions at the necessary values.

It is possible to illustrate the adequacy of these fragmentation functions by comparing them with data on the z distributions of charged hadrons as measured both in high Q^2 e^+e^- annihilation and in high-p_T jet production. In Fig. 4 the predictions based on the above simple
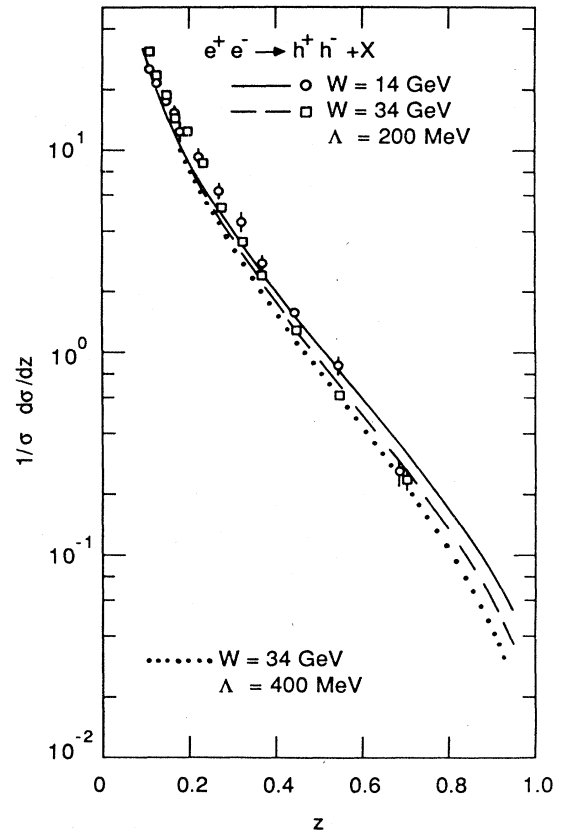

FIG. 4. Comparison between the predictions of the simple fragmentation functions discussed in the text and data on hadron production in e^+e^- annihilation from Althoff et al. (1984).

fragmentation functions are compared with the charged-hadron z distributions obtained by the Tasso Collaboration (Althoff et al., 1984). Although the good agreement is encouraging, a number of cautionary comments are necessary. First, the amount of scaling violation shown can also be described by a model that incorporates mass effects as well as some transverse momentum in the fragmentation process. Therefore the observed scaling violations may not really be testing the perturbative evolution. Second, heavy-quark production has not been included in the theoretical curve, even though this accounts for a large part of the cross section. However, as a result of the heavy flavor decays, these effects contribute to a lower region of z than is required for high-p_T particle production, for which it is the high-z region that is most important. Thus the agreement shown in Fig. 4 indicates that the fragmentation functions should be adequate for studying quantities that depend on the z dependence of particle production in the high-z region. This point is strengthened by the results shown in Fig. 5, which is a comparison of high-p_T jet fragmentation data with predictions based on the simple fragmentation functions. The data shown by the solid circles are from the AFS Collaboration (Åkesson et al., 1984) and were obtained at the intersecting storage rings (ISR) using proton-proton
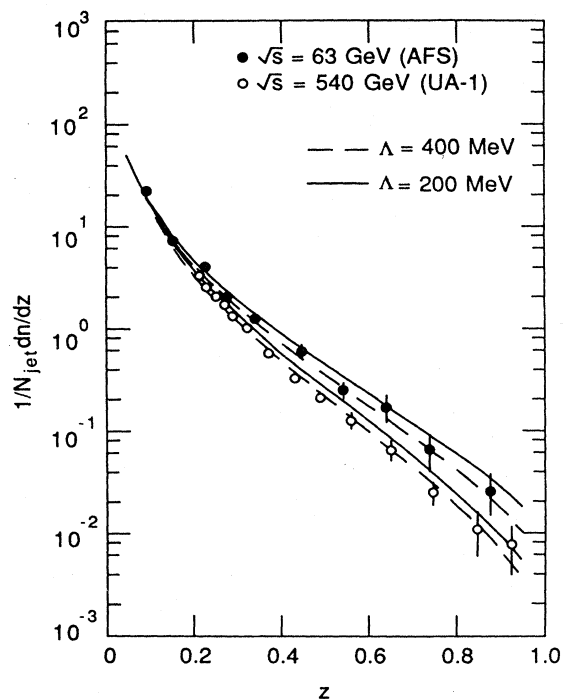
FIG. 5. Comparison between the predictions of the simple fragmentation functions discussed in the text and data for jet fragmentation from the AFS Collaboration (Åkesson *et al.*, 1984) and from the UA-1 Collaboration (Arnison *et al.*, 1986b).

collisions at $\sqrt{s} = 62.4$ GeV. At this energy, and in the p_T range studied, the dominant process should be quark fragmentation. On the other hand, at the energies available at the CERN $Sp\bar{p}S$ Collider—$\sqrt{s} = 540$–630 GeV—the jets in the p_T region around 30–60 GeV should result predominantly from gluons. The data shown by the open circles in Fig. 5 are from the UA-1 Collaboration (Arnison *et al.*, 1986b) and are for jet fragmentation at an average p_T of 36 GeV. The steepening of the z distribution is well described by the simple fragmentation functions and is due both to the perturbative evolution and to the fact that the input gluon fragmentation function was chosen to be slightly steeper than the valence quark fragmentation functions. It should be noted that data from a more recent run at the ISR by the AFS Collaboration (Åkesson *et al.*, 1986a) show a somewhat harder frag-

mentation function than that shown by the solid circles in Fig. 5. However, the two data sets are consistent once the systematic errors are taken into account.

Taken together, the results in Figs. 4 and 5 lend support to the idea that the simple fragmentation functions discussed here are adequate for describing those distributions in high-p_T processes that deal with one- or two-particle distributions.

In the preceding section it was briefly mentioned that direct photons are produced primarily through the two subprocesses $qg \rightarrow q\gamma$ and $q\bar{q} \rightarrow g\gamma$. In addition, however, one must also consider the possibility of bremsstrahlung from the quarks participating in the hard scattering. The photon couples to the electric charge of the quarks, and the resulting pointlike vertex is the same as in quantum electrodynamics. Thus the effective fragmentation functions for obtaining photons from partons can be calculated. The resulting expressions are

$$zD_{\gamma/q_i}(z,Q^2) = e_i^2 \frac{\alpha}{2\pi}[1 + (1-z)^2]\ln(Q^2/\Lambda^2) \qquad (6a)$$

and

$$zD_{\gamma/g}(z,Q^2) = 0 , \qquad (6b)$$

where e_i is the fractional charge of the ith quark. In the derivation of Eq. (6) an integration must be performed over the transverse momentum of the photon with respect to the quark. The upper limit for this integration has been taken to be the typical hard-scattering momentum scale Q^2 discussed previously. The divergence associated with the lower limit is regulated for massive quarks by the quark mass itself. However, for massless quarks some infrared cutoff is needed. The size of this cutoff should be that of some characteristic hadronic scale. In Eq. (6a) the cutoff has been replaced by the QCD scale parameter Λ. The leading logarithm terms are unaffected by this replacement. Other choices would affect only the nonleading logarithms, and, as such, would be beyond the leading-logarithm approximation.

The photon fragmentation functions evolve with Q^2 just as the usual hadronic fragmentation functions do, as a result of gluon bremsstrahlung and $q\bar{q}$ pair production. The result is a softening of $D_{\gamma/q}$ and the introduction of a new fragmentation function $D_{\gamma/g}$, which was previously zero. The Q^2 evolution can be derived from a set of coupled equations similar to Eq. (5), but with an added term, $P_{\gamma/q}$, that describes the splitting $q \rightarrow \gamma q$. The resulting evolution equations are

$$\frac{dD_{\gamma/q_i}(z,Q^2)}{dt} = \frac{\alpha}{2\pi}e_i^2\frac{1+(1-z)^2}{z} + \frac{\alpha_s(Q^2)}{2\pi}\int_z^1 \frac{dy}{y}[D_{\gamma/q_i}(y,Q^2)P_{qq}(z/y) + D_{\gamma/g}(y,Q^2)P_{gq}(z/y)] \qquad (7a)$$

and

$$\frac{dD_{\gamma/g}(z,Q^2)}{dt} = \frac{\alpha_s(Q^2)}{2\pi}\int_z^1 \frac{dy}{y}\left[\sum_{i=1}^{2f} D_{\gamma/q_i}(y,Q^2)P_{qg}(z/y) + D_{\gamma/g}(y,Q^2)P_{gg}(z/y)\right] . \qquad (7b)$$

These evolution equations are very similar to those used to derive the evolution of the parton distributions in a photon (DeWitt, Jones, Sullivan, Williams, and Wyld, 1979) and can be solved in a similar manner. For each distribution there is a leading term that is proportional to $\ln(Q^2/\Lambda^2)$, and the functional form of the coefficient can be calculated using the above equations. However, in order to solve completely for the fragmentation functions, one must specify the appropriate boundary conditions for Eq. (7). These will contribute nonleading terms and must be taken either from data or from some set of model-dependent assumptions. The corresponding problem for the distribution functions of partons in a photon (the photon structure function, in other words) has been discussed extensively in the literature (Bardeen, 1984; Glück, Grassie, and Reya, 1984; Owens, 1985b).

The reason for going into such detail concerning the photon fragmentation functions is their logarithmic growth with Q^2. Put another way, the photon fragmentation functions are proportional to $\alpha/\alpha_s(Q^2)$. Now, the lowest-order two-body subprocesses are proportional to $\alpha\alpha_s$, whereas the two-body parton-parton subprocesses are proportional to α_s^2. However, if one convolutes the parton-parton subprocesses with the fragmentation function of a parton to a photon, the resulting contribution is of order $\alpha\alpha_s$. Therefore it is conceivable that the bremsstrahlung photons could be produced at a rate comparable to those coming from the annihilation and Compton subprocesses. This is a point of some importance, since the underlying parton kinematics is quite different for the two cases.

In the following, I shall use the leading term for each of the fragmentation functions that results from solving Eq. (7). The subleading terms coming from imposing boundary conditions at some Q_0^2 will not be included, since the relevant data are not available. However, experience with the corresponding problem in the case of the photon structure function suggests that the leading term will be approached from below in the high-Q^2 limit and that, therefore, the predictions for the bremsstrahlung component to be presented later are actually overestimates.

It is useful to have some simple parametrizations for the photon fragmentation functions. The following set is compact and accurately reproduces the exact leading-logarithm solution:

$$zD_{\gamma/q_i}(z,Q^2) = \frac{\alpha}{2\pi}\left[e_i^2 \frac{2.21-1.28z+1.29z^2}{1-1.63\ln(1-z)}z^{0.049}\right.$$

$$\left. +0.002(1-z)^2 z^{-1.54}\right]\ln(Q^2/\Lambda^2) \quad (8a)$$

and

$$zD_{\gamma/g}(z,Q^2) = \frac{\alpha}{2\pi}0.0243(1-z)z^{-0.97}\ln(Q^2/\Lambda^2) . \quad (8b)$$

In Fig. 6 the results from Eq. (8) are shown for both the gluon and the u quark. For comparison the results of
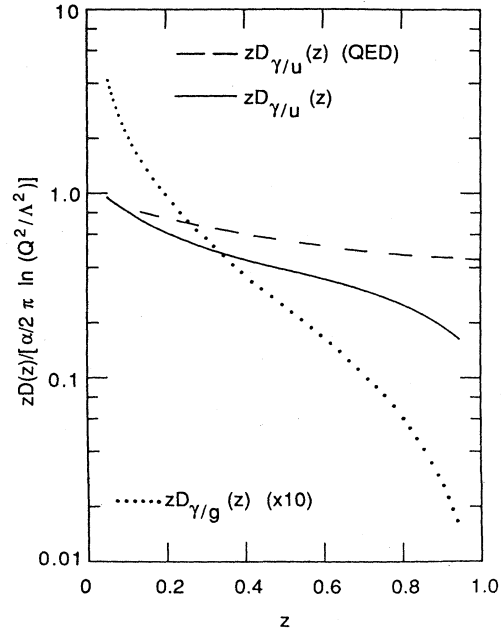

FIG. 6. Photon fragmentation functions: lowest-order QED prediction for u-quark fragmentation (dashed curve); leading-logarithm QCD prediction for u-quark fragmentation (solid curve); leading-logarithm QCD prediction for gluon fragmentation (dotted curve). For ease of plotting, the gluon curve has been multiplied by 10. A common scale factor and the logarithmic Q^2 dependence have been divided out.

Eq. (6) are shown for a u quark as well. In all three cases an overall factor of $\ln(Q^2/\Lambda^2)$ has been removed. It is clear that whereas the Q^2 dependence is the same in both Eqs. (6) and (8), the shapes of the quark fragmentation functions are quite different. The QCD evolution (due primarily to gluon bremsstrahlung) has considerably softened the quark fragmentation function in the high-z region. The evolution has also given rise to a small gluon fragmentation function, but one can see that it is suppressed to a large extent in the high-z region, which, after all, is the dominant region for high-p_T photon production. These results will be used in Sec. III, where the relative rates of the bremsstrahlung, Compton, and annihilation terms will be discussed.

C. Higher twist contributions

The two-body subprocess cross sections listed in Table I all have in common the feature that dimensionally they are proportional to GeV^{-4} and that this dimension must be supplied by some combination of $\hat{s}$, $\hat{t}$, and $\hat{u}$. This follows from the fact that the relevant strong and electromagnetic couplings are dimensionless and that there is no other mass scale for the subprocesses, the partons always being treated as massless. When combined with Eq. (1), this result allows one to construct a scaling relationship for the invariant cross section. This may be done

equally well for jets, hadrons, or photons—I shall use photons for the purpose of this discussion. The invariant cross section depends, in general, on three kinematic variables. These can be chosen in such a way that two are dimensionless, e.g., s, x_T, and θ or, equivalently, p_T, x_T, and θ. If we consider the behavior of the invariant cross section when the two dimensionless variables are held constant, then the dimensionality argument given above allows us to determine the dependence on the third (dimensioned) variable. Specifically we can write

$$E\frac{d^3\sigma}{dp^3}(AB\to\gamma+X)=\frac{F(x_T,\theta)}{p_T^n} \qquad (9)$$

with $n=4$ and where $F(x_T,\theta)$ is a dimensionless function. However, when one makes the transition from the parton model to QCD perturbation theory, as embodied in Eq. (4), the simple dimensional arguments no longer hold. The QCD scale parameter Λ, whose existence can be traced back to the need for specifying a renormalization point that has the dimensions of a momentum, allows for more complicated dependences on the kinematic variables. Specifically, there is the logarithmic dependence on the factorization scales and the logarithmic dependence on the argument of the running coupling. Both of these logarithmic dependences tend to enhance the rate of decrease of the cross section with increasing p_T. That is, the power of 4 in Eq. (9) is increased somewhat, the exact amount depending on the kinematic region and the actual reaction considered. The effect is largest for hadron production because of the extra scale violation associated with the fragmentation functions, and it is smallest for direct-photon production because there is one less factor of α_s.

Experimentally, it was observed that the data for high-p_T meson production obeyed Eq. (9) rather well, provided that $n=8$ was used. The scaling violations could, at most, raise the value of n from 4 to approximately 6. The net result was that the cross section was underestimated theoretically in the region of p_T below about 7 GeV, for $\sqrt{s}$ in the ISR range or below, i.e., below about 60 GeV. One method of resolving this disagreement would be to have additional production mechanisms that obeyed scaling laws different from those of the simple two-body subprocesses discussed thus far. One such model was proposed by Blankenbecler, Brodsky, and Gunion (1972, 1973, 1975) and was termed the Constituent Interchange Model, or CIM. The application of this model to high-p_T processes is reviewed in detail by Sivers, Brodsky, and Blankenbecler (1976) and Blankenbecler, Brodsky, and Gunion (1978). The CIM is characterized by subprocesses that involve composite objects, e.g., mesons, baryons, and diquarks, in addition to quarks and gluons. The original CIM calculations contained phenomenological couplings that carried dimensions and that therefore resulted in subprocesses obeying different scaling laws. In Jones and Gunion (1979) it was demonstrated that a consistent description of the high-p_T meson and baryon production data could be obtained by combining the various CIM

subprocesses (such as $Mq\to Mq$, $q\bar{q}\to MM$, etc., where M stands for a meson) with the lowest-order QCD subprocesses discussed above. This same approach was applied to direct-photon production in Horgan and Scharbach (1981) and in Rückl, Brodsky, and Gunion (1979).

The existence of these additional subprocesses gives rise to new types of quantum number correlations. For example, the presence of the $\pi^-q\to\pi^-q$ subprocess gives rise to a large π^-/π^+ cross-section ratio in π^-p interactions that increases with increasing transverse momentum (Jones and Gunion, 1979). Such correlations were sought, but effects of the predicted size were not found (Frisch et al., 1980). Subsequently, techniques were developed for calculating the normalizations of the CIM subprocesses within QCD, and the phenomenological couplings were found to give contributions that were of order 10^3 times too larger (Farrar and Fox, 1980). In Berger, Gottschalk, and Sivers (1981) a similar but more detailed study of the dominant CIM terms was made. Their conclusion was that the CIM terms could have a significant effect in the region of $p_T\leq6$ GeV/c with $x_T\geq0.5$. This region lies outside that covered by presently available data. While these studies resolved the question of the quantum number correlations by lowering the normalization of the CIM terms, there remained the need for a solution to the problem of the scaling behavior. More will be said about this point later.

This capsule summary of the history of CIM calculations is meant only to serve as an introduction to the present-day higher twist calculations and does not adequately reflect the huge amount of theoretical and experimental effort that have been devoted to this topic. The interested reader is referred to the literature listed above.

The current terminology for the types of subprocesses that used to comprise the CIM is "higher twist"—a phrase that, itself, is a relic of the past when the operator product expansion was the chief tool for obtaining perturbative QCD predictions for deep-inelastic scattering. Simply stated, the term as used today refers to contributions that are suppressed by powers of large momenta with respect to the leading terms. This power-law suppression is to be distinguished from the logarithmic modifications that have been discussed above.

For reactions involving photons, several calculations have been performed for subprocesses for which the normalization can be calculated in terms of experimentally measured quantities. Specifically, calculations have been performed using the subprocess $\gamma q\to\pi q$ (Bagger and Gunion, 1982) in a study of the relative sizes of the higher twist and leading twist terms in high-p_T photoproduction. The time-reversed subprocess $\pi q\to\gamma q$ was used in a similar study for direct-photon production (Berger, 1982). Both of these calculations start by assuming a model for the pion wave function $\phi_\pi(x,Q^2)$, which is defined as the probability amplitude for finding a quark and an antiquark in the pion with momentum fractions x and $(1-x)$, respectively, and which are collinear up to transverse momenta of order Q. ϕ_π can be related to the pion electromagnetic form factor F_π:

$$Q^2 F_\pi(Q^2) = \tfrac{4}{3}\pi C_2(R)\alpha_s(Q^2) \left| 2 \int \frac{dx}{1-x} \phi_\pi(x,Q^2) \right|^2 .$$

The asymptotic form of the pion form factor can be calculated, and some data exist at relatively low Q^2, as well. Therefore, it is possible to obtain a model-dependent estimate for the pion wave function ϕ_π (Bagger and Gunion, 1982; Lepage and Brodsky, 1980). The invariant cross section for direct-photon production takes the form (Berger, 1982)

$$E\frac{d^3\sigma}{d^3 p_\gamma} = \sum x G_{q_i/N}(x,Q^2)\frac{s}{s+u}\frac{1}{\pi}\frac{d\sigma}{d\hat{t}}(\pi q \to \gamma q) ,$$

(10a)

where the subprocess cross section is given by

$$\frac{1}{\pi}\frac{d\sigma}{d\hat{t}} = \frac{4}{9}\alpha\alpha_s F_\pi(\hat{s}) \left[\frac{1}{\hat{u}^2} + \frac{1}{\hat{s}^2} \right] \frac{(e_2\hat{s}+e_1\hat{u})^2}{-\hat{t}\hat{s}} .$$

(10b)

Here e_1 and e_2 label the quark (not antiquark) electric charges in the pion.

In Eq. (10b) the presence of the pion form factor gives an extra factor of $\hat{s}$ in the denominator. This gives rise to a p_T^{-6} scaling form in the sense of Eq. (9). One might expect this contribution to dominate those of the Compton and annihilation graphs (the so-called leading twist terms) at sufficiently small p_T. In addition, notice that in Eq. (10a) there is only one structure function, whereas the two-body leading twist subprocesses all involve two structure functions in the initial state. The structure functions typically fall off as a power of $(1-x)$, the precise exponent depending on the parton flavor and the type of parent hadron. Furthermore, the argument x goes smoothly to 1 as the edge of phase space is approached. In this region, therefore, the leading twist terms are suppressed by an additional factor of $(1-x)$ to a power, relative to the higher twist contribution.

I have used the pion wave function given in Bagger and Gunion (1982) to estimate the size of the higher twist contribution relative to that for the leading twist terms. At $\sqrt{s} = 31$ GeV for $\theta = 90°$ and p_T below about 7 GeV, the higher twist contribution is suppressed by about 2 orders of magnitude relative to the leading twist predictions to be discussed in Sec. III. However, as one approaches the edge of phase space, the leading twist contribution steepens and that of the higher twist term flattens, leading to an eventual crossover, as expected. This crossover is in a region where x_T near 1 and the cross section is extremely small. It is therefore likely that a careful study of specific triggers that exploit the characteristic signatures of the higher twist subprocesses will be required in order to separate the two contributions. Additional discussion of the phenomenology of the higher twist terms can be found in Berger (1982). There the relative suppression between the two types of terms is somewhat less than that quoted above, since not all of the possible contributions from the leading twist terms have been included. However, the trend is the same.

One may wonder whether there are any other higher twist contributions that could make significant contributions. The crossed subprocess $q\bar{q} \to \gamma M$ will be suppressed by a combined spin and color factor of $\tfrac{1}{6}$. Moreover, the presence of a second structure function in the initial state provides further suppression. Terms involving diquarks, such as $\bar{q}(qq) \to \gamma q$, will be similarly suppressed. Furthermore, the normalization is not easily calculated for the diquark subprocesses.

At this point it appears as if the higher twist terms do not make significant contributions in the regions where data are available. However, they can become important near the edge of phase space, and their effects have been found in several recent experiments. For example, in high-mass dimuon production by pions the polarization of the dimuon system is predicted to have a strong variation as $x_F \to 1$ (Berger and Brodsky, 1979; Berger, 1980a, 1980b) due to the presence of higher twist subprocesses $\pi q \to \gamma^* q$. Several experiments have now detected this effect (Anderson et al., 1979; Palestini et al., 1985). A second example is in the production of jets by pion beams. The subprocess $\pi q \to gq$ produces events with two high-p_T jets and few forward-going particles, i.e., the usual beam jet is missing. Evidence for events of this type has recently been reported by the E-609 Collaboration (Naudet et al., 1986).

In summary, there is mounting evidence for higher twist effects near the edge of phase space and at approximately the expected level. Whereas these effects are too small to be detected in the kinematic regions covered by current direct-photon data, it may be possible to find them with a high-statistics experiment and a specialized trigger.

D. k_T smearing

In the previous discussion it was pointed out that the original leading-logarithm calculations for high-p_T hadron production all gave results that were below the data in the p_T region below about 7 GeV, for $\sqrt{s}$ below about 60 GeV. Furthermore, the scaling law obeyed by the data, which clearly showed $n = 8$ for meson production, did not agree with the leading-logarithm QCD predictions, which gave $n \approx 6$. The CIM subprocesses were discussed as one possible way of simultaneously solving both of these deficiencies. A second attempt centered on the idea that the colliding partons might have some initial transverse momentum k_T with respect to the incoming hadrons. This analog of the Fermi motion of nucleons in a nucleus would give rise to a smearing out of the p_T spectrum. Since the invariant cross section falls at the rate of an order of magnitude per GeV of p_T in this region; it would not take a large amount of smearing to make a significant effect. There could also be an additional smearing due to the k_T associated with the fragmentation in the final state.

The steeply falling single-particle spectrum results from a number of different factors. First, for collinear interac-

tions, as the transverse momentum of the observed particle is increased, the minimum values of $\hat{s}$, $\hat{t}$, and $\hat{u}$ all increase in magnitude. Thus the cross sections for the individual subprocesses decrease. Second, the minimum values of x_a and x_b [see Eq. (A5)] also increase. This occurs in a region in which the parton distribution functions are rapidly decreasing functions of x. Finally, the average value of z in the fragmentation increases with increasing transverse momentum, which leads to an additional decrease of the cross section from the fragmentation functions. The net result of these effects is the rapid falloff seen in both the data and the calculations.

Now, suppose that the initial partons are not quite collinear with the beam and target axis, i.e., that the initial partons themselves have some transverse momentum k_T. Since part of the total transverse momentum is supplied by the initial quarks themselves, the amount supplied by the hard scattering is decreased. Thus the existence of k_T can lead to an increase in the cross section. (If a single-arm trigger is used, it will preferentially select those events in which the initial quarks already had some transverse momentum toward the detector. This phenomenon is sometimes referred to as "trigger bias.")

As discussed above, the problem in the moderate-p_T region is not so much that the cross section is too low, but rather that the scaling behavior is wrong. Consider what happens when p_T is increased while x_T is held constant. The x_a and x_b integration ranges stay the same while both p_T and s are increased. Therefore, as can be seen from the kinematics in the Appendix, the minimum values of $\hat{s}$, $\hat{t}$, and $\hat{u}$ also increase. Suppose that the parton k_T distribution is assumed to arise via the uncertainty principle and the fact that the partons are confined within the hadrons. In this case the average value of the parton transverse momentum would be set by a characteristic hadronic size and the distribution would not change with s. This would mean that the effect of the smearing on the parton Mandelstam variables would become less pronounced as s increased at fixed x_T. But this means that the cross section would fall more rapidly with increasing p_T (or s) at fixed x_T than if the smearing were not present at all. Therefore the scaling exponent n in Eq. (9) would be increased. It is for this reason that various models for the inclusion of these "intrinsic" transverse-momentum effects have been proposed. Phenomenological studies of these effects include, for example, those of Feynman, Field, and Fox (1978), Owens and Kimel (1978), and Field (1979).

In the parton model approach it is assumed that the average value of the intrinsic transverse momentum reflects the size of the hadron via the uncertainty principle. This leads to the expectation that $\langle k_T \rangle$ may be in the range of several hundred MeV. This is in accordance with the observation that inclusively produced pions have an average p_T of about 300 MeV. This simple idea is complicated by the fact that there are other sources of parton transverse momenta as soon as one considers the various subprocesses given by QCD. For example, the $2 \rightarrow 3$ subprocesses with an additional radiated gluon give rise to the same type of effect as discussed above. In fact, it is difficult theoretically to separate the intrinsic k_T from the radiative corrections, since they ultimately come from the same source—quark and gluon interactions.

A particularly good reaction for studying these transverse-momentum effects is high-mass lepton pair production. The lowest-order subprocess is $q\bar{q} \rightarrow l^+ l^-$. If only this subprocess is used, the transverse momentum of the lepton pair gives a direct measure of the intrinsic parton transverse momentum. For example, data at $\sqrt{s} = 27.4$ GeV (Kaplan et al., 1978) indicate $\langle p_T^2 \rangle = 1.9$ GeV^2. This corresponds to an intrinsic $\langle k_T^2 \rangle$ of 0.95 GeV^2 or, assuming a Gaussian shape; $\langle k_T \rangle = 864$ MeV—clearly larger than expected. However, the next-order subprocesses—$gq \rightarrow l^+ l^- q$ and $q\bar{q} \rightarrow l^+ l^- g$—will give rise to a lepton pair transverse-momentum distribution with a characteristic p_T^{-4} tail at high values of p_T. If these terms are included, then the value of the intrinsic k_T is reduced to about 600 MeV (Field, 1978). The convolution is, however, a model-dependent prescription for incorporating the effects of the intrinsic k_T. Nevertheless, this example demonstrates that the amount of intrinsic k_T needed to describe the data is strongly affected by the amount of QCD dynamics included in the calculation. In general, as more calculable QCD terms are included, the size of the deduced intrinsic term is decreased.

Those who are interested in studying this issue in more detail should consult the papers of Altarelli, Ellis, Greco, and Martinelli (1984) and Collins, Soper, and Sterman (1985), in which a complete formalism for describing the lepton pair p_T distribution has been worked out.

In addition to the theoretical problems of defining "intrinsic transverse momentum," there are also ambiguities in how one incorporates the distributions into a specific calculation. Various assumptions must be made, and this introduces a certain amount of model dependence into the calculations. In what follows I shall describe a particular way of handling the k_T smearing, but it is by no means a unique description. The first step is to make the following replacement in Eq. (4),

$$dx_a G_{a/A}(x_a, Q^2) \rightarrow dx_a d^2 k_{Ta} f(\mathbf{k}_{Ta}) G_{a/A}(x_a, Q^2) , \qquad (11)$$

where the distribution $f(\mathbf{k}_{Ta})$ is taken to be of the form

$$f(\mathbf{k}_{Ta}) = \frac{e^{-k_T^2/\langle k_T^2 \rangle}}{\pi \langle k_T^2 \rangle} , \qquad (12)$$

for which the relation $\langle k_T^2 \rangle = 4 \langle k_T \rangle^2 / \pi$ is satisfied. A substitution of the same form as Eq. (11) is also made for parton b.

Having made the assumption that the intrinsic transverse-momentum distribution can be factored out of the longitudinal distribution as shown in Eq. (11), we need next to decide how to construct the four-vectors of the colliding partons. The prescription that I shall use is to define the momentum fraction x in terms of the light-cone variables. If we ignore parton and hadron masses, then

$$x_a = (E_a + p_{al})/\sqrt{s} \; ,$$

and the parton four-vector is

$$p_a = (E_a, \mathbf{k}_{Ta}, p_{al}) \; ,$$

with

$$E_a = \frac{1}{2} \left[x_a \sqrt{s} + \frac{k_{Ta}^2}{x_a \sqrt{s}} \right]$$

and

$$p_{al} = \frac{1}{2} \left[x_a \sqrt{s} - \frac{k_{Ta}^2}{x_a \sqrt{s}} \right] \; .$$

Similar expressions exist for partons b and c, except that allowance must be made for the fact that the longitudinal momentum of b is in the opposite direction from that of a.

With these expressions it is reasonably straightforward to evaluate the invariant cross section with k_T effects included. The invariant cross section for hadron production now involves an eight-dimensional integration, so that Monte Carlo techniques are usually employed. There are several subtleties left to discuss, however. In the formulation shown above, it is possible for p_{al} to become negative if $|\mathbf{k}_{Ta}|$ exceeds $x_a \sqrt{s}$. Such events must be discarded in the evaluation of the integral, since this corresponds to having the parton going toward the wrong hemisphere. Also, if the k_T's become too large, one or more of the Mandelstam variables can approach zero, and excessively large weights will then be generated. This corresponds to a situation in which the large transverse momentum is being generated by fluctuations in the intrinsic k_T distribution and not by the hard scattering itself. Such a situation is difficult to reconcile with the use of perturbation theory, in which α_s is assumed to be small due to the presence of the large momentum transfer. The cutoff procedure mentioned above avoids this problem. An alternative method for avoiding the s-, t-, and u-channel singularities is to give the partons an off-shell mass proportional to k_T^2 (Caswell, Horgan, and Brodsky, 1978). The expression for this off-shell mass can be derived by working out the kinematics for a massless parton splitting into another massless parton plus one that is off-shell and has a transverse momentum $\mathbf{k}_T$ with respect to the initial parton. This procedure is often referred to as off-shell kinematics, whereas the procedure discussed previously uses on-shell kinematics throughout. In actual practice, if one uses some cutoff scheme in order to avoid the propagator poles and if $\langle k_T \rangle$ is not too large, the various schemes yield similar results.

In Sec. III a detailed comparison between the theoretical predictions and the data will be presented. At that time the effects of the on-shell k_T-smearing approach will be discussed further.

E. Next-to-leading-order calculations

Up to this point in the review the contributions from subprocesses with more than two partons in the final state

have been treated only in the leading-logarithm approximation. Before discussing the nature of the higher-order calculations, a few comments concerning terminology may prove helpful. The leading-logarithm calculations discussed thus far have been based on the factorization ansatz implicit in Fig. 1. The hard-scattering subprocess is calculated using perturbation theory. The first term in the series will start with a characteristic power of α_s, e.g., α_s^2 for two-body parton scattering. All higher-order subprocesses, i.e., those with more than two partons in the final state, are treated in the leading-logarithm approximation, and the results are incorporated into the various scale-dependence distribution and fragmentation functions. In addition, the one-loop expression for the running coupling is used. This procedure represents an all-orders calculation, but one in which only the leading-logarithm terms are retained. In this approximation, the additional partons, beyond those present in the lowest-order term, are parallel to the beam, target, trigger, or recoil directions. Therefore the kinematics is unchanged from that used for the lowest-order calculation. The next step in improving upon the leading-logarithm approximation would be to retain all those terms which are suppressed by one power of a large logarithm with respect to the leading logarithm terms. Such a calculation also includes terms with no large logarithms. These are sometimes referred to as the "constant pieces." To do this requires that the next term in the hard-scattering series be calculated exactly. In the case of parton-parton scattering, this means calculating the $O(\alpha_s^3)$ contribution. Thus such a calculation is sometimes referred to as a next-to-leading-order calculation. The result obtained is equal to the leading-logarithm result plus all the next-to-leading logarithm terms (including the constant pieces) and is therefore sometimes referred to as a next-to-leading-logarithm calculation. However, both terms refer to the same type of calculation.

There are at least two reasons for wanting to calculate the next-to-leading logarithm terms. The first has to do with the appropriate choices for the factorization scales and the argument of the running coupling, and the second is related to the question of whether or not the perturbation series is converging. As was discussed earlier in this section, the parton distribution and fragmentation functions must be defined using some suitable reference processes. Furthermore it is necessary to specify the factorization scales in terms of the kinematic variables for the reaction being studied. These two steps together constitute a specific *factorization prescription*. A detailed study of the effects of various prescription choices is contained in the article of Celmaster and Sivers (1982), where additional references to this subject may be found. In addition to the factorization prescription, a *renormalization scheme* must also be chosen in order to treat the ultraviolet singularities that arise from loop graphs such as those in Fig. 2(e). The specific choice made will, in turn, serve to define the running coupling α_s. If, in the calculation of some process, all orders of perturbation theory were retained without approximation, then the final answer

would be independent of the various choices made for the factorization prescription and the renormalization scheme.

In the leading-logarithm approximation we have seen that there is an equivalence among all "large scales." However, this equivalence is only a formal one, and the actual numerical value of the result often depends quite strongly on the choices made. When the next-to-leading logarithm terms are retained, some of this sensitivity is reduced, since a change in the factorization scale is partially compensated by the subleading logarithms. Indeed, one method for specifying the factorization scale is to choose the definition that minimizes this sensitivity (Stevenson, 1981a, 1981b). In addition, there is no dependence on the renormalization convention at the leading-logarithm level. In order to determine the QCD scale parameter Λ in a particular renormalization scheme (MS, MOM, etc.), at least the next-to-leading terms must be calculated.

The second, related point concerns the convergence of the perturbation series. In some instances the series appears to be under control, in the sense that the next term in the perturbation expansion is sensibly small with respect to that which precedes it. However, there are well-known cases in which the corrections are quite large. One such example is the production of lepton pairs in which the next-to-leading-logarithm calculation yields a contribution nearly as large as the leading one. A terminology has evolved whereby this is usually described in terms of a "K factor," the precise definition of which varies to some extent. Since the term has different meanings for different people, I shall refrain from using it wherever possible. However, it will occasionally be necessary to discuss results quoted in terms of a K factor. For the purpose of this review I shall define it in the following way. Write the perturbation series result for some process at the parton level as

$$\sigma_0 + \alpha_s \sigma_1 + \cdots = K \sigma_0 , \qquad (13)$$

so that the deviation of K from 1 gives a measure of the importance of the higher-order terms in the series. In the lepton pair production example the next-to-leading terms alone give rise to a K factor of approximately 2, making it difficult to have much faith in the convergence of the series. It appears, however, that at least a portion of the perturbative correction can be exponentiated, with the remaining corrections being relatively small. This question of exponentiation has recently been discussed by Sterman (1986, 1987). A review of earlier work can be found in these references as well.

A complete next-to-leading-logarithm calculation exists for the single-photon inclusive invariant cross section (Aurenche, Douiri, Baier, Fontannaz, and Schiff, 1984, 1985). A selection of the graphs considered is shown in Fig. 2. This calculation includes all subprocesses in which the photon interacts directly in the hard scattering. In principle, one should also include all possible $2 \rightarrow 3$ order α_s^3 subprocesses convoluted with the order α / α_s photon fragmentation functions. These contributions have not been included in the present calculation. The calculation of all $2 \rightarrow 3$ parton subprocesses by Ellis and Sexton (1986) now makes this a straightforward, although lengthy, task. However, the neglect of these terms is not unreasonable, since they are corrections to the bremsstrahlung contribution, which is already rather small.

1. Complete calculations

In order to understand some elements of the next-to-leading-order calculations to which we shall refer later, it will be useful to outline the procedures utilized in such a calculation. This discussion will be extremely brief, and additional details can be found, for example, in the paper of Buras (1980). The graphs shown in Fig. 2(e) give rise to a variety of infrared and ultraviolet singularities, which must be regularized or rendered finite. The most common procedure utilized today is called dimensional regularization ('t Hooft and Veltman, 1972). This method is easy to implement and has the technical virtue of being a gauge-invariant regularization scheme. The calculation is first performed in $n = 4 - 2\varepsilon$ space-time dimensions, which converts the logarithmic singularities into poles in ε. The ultraviolet singularities thus isolated can be subtracted off once a specific renormalization scheme has been chosen. Subsequently, the infrared singularities associated with the virtual graphs [such as Fig. 2(e)] are canceled by corresponding singularities in the tree graphs [such as Fig. 2(c)]—in QED this is a consequence of the Bloch-Nordsieck theorem (Bloch and Nordsieck, 1937). Finally, the collinear singularities, which give rise to the scaling violations in the distribution and fragmentation functions, must be removed. Their effects are already included in the leading-logarithm portion of the calculation. The result remaining after this procedure constitutes the next-to-leading-logarithm contribution. The relative size of this contribution, with respect to that of the leading terms, is controlled, in part, by the choices made for the factorization and running coupling scales. Indeed, different choices can even lead to a change of sign for the next-to-leading terms. The dependence on the choices for these scales can be exploited in a variety of ways. For example, it may be possible to find a range of values for the scales over which the total result shows little variation. This represents an approximation to the stability, which should be possessed by an exact, all orders calculation. It may also be possible to choose the scales in such a way that the next-to-leading contribution becomes zero. In practice, these two schemes often yield very similar results for the final answer. Specific examples will be presented in Sec. III.

2. K factors and soft gluons

The calculation of the next-to-leading-order corrections is a rather lengthy process, which often results in cumbersome expressions involving many terms. Approximate methods that would at least indicate whether large pertur-

bative corrections are present in a given process have, therefore, been sought. One such approach (Contogouris, Papadopoulos, and Ralston, 1981, 1982) makes use of the fact that the largest corrections are often associated with virtual diagrams that can give rise to terms containing factors of π^2. These result from the analytic continuation of various logarithms from spacelike to timelike regions. This particular class of terms can be calculated in what is known as the "soft-gluon approximation." As mentioned above the singularities associated with the virtual graphs are canceled by singularities coming from tree graphs. The relevant tree-graph singularities originate from a region in phase space corresponding to vanishing momenta for the unobserved final-state gluons. It is possible to make a systematic expansion of the various integrands, dropping terms that are proportional to positive powers of the vanishing gluon momenta. This results in a considerable simplification, and the full result is proportional to just the lowest-order term. A second type of π^2 term is associated with soft collinear gluon bremsstrahlung and can be calculated in an approximate manner (Contogouris, 1982). A systematic study of such terms has been presented by Contogouris and Tanaka (1985, 1986). They find that the answer is always of the form

$$\sigma = \sigma_0[1 + \alpha_s(Q^2)C] \; , \tag{14}$$

where C is a subprocess-dependent constant. The proponents of this approach claim that one can reliably determine which reactions are going to have large next-to-leading-order corrections and, further, that the magnitude of the corrections can be approximately determined. A survey of results (Contogouris and Tanaka, 1986) obtained for processes involving real photons offers some support to this contention, although not without qualification.

There is, however, a basic limitation to this approach. The simple form shown in Eq. (14) does not contain the full dependence on the renormalization or factorization schemes that is found in the complete next-to-leading-order calculation. Therefore it is not possible to use the soft-gluon results in a systematic program for measuring Λ in a particular renormalization scheme. Furthermore there is no way to use one of the optimization techniques to determine the factorization scale.

For some processes the complete next-to-leading-order calculations have been performed. It has, therefore, been possible to compare the exact results with those from the soft-gluon approximation. The two sets of results are often in reasonable agreement, provided that the factorization and running coupling scales are chosen to be equal to a large momentum that is characteristic of the process, e.g., p_T^2 in the case of direct-photon production (Contogouris and Tanaka, 1986). Of course, if one has the complete calculation available, the relative size of the leading and next-to-leading terms can be varied by choosing different scales, while the same is not true in the soft-gluon approach. It is for this reason that some care must be used when interpreting the soft-gluon results.

In many cases the soft-gluon "K factors" lead to an increase of the leading-logarithm predictions by a factor of about 2. Such a variation can also be achieved by reasonable variations in the choice of the factorization and running coupling scales. Specific examples will be presented in the next section.

At this point all of the major ingredients of typical QCD calculations for high-p_T processes have been covered. In the next section specific examples of such calculations will be compared with data. Special attention will be devoted to the topics discussed in this section, such as the choice of the factorization scales, the effects of nonleading logarithms, and k_T smearing.

III. COMPARISON WITH DATA

A. Jet and single-particle cross sections

Having reviewed the basic formalism for calculating cross sections for high-p_T processes, it is now time to compare the theoretical results with the data. At first this comparison will be restricted to predictions based on the leading-logarithm approximation. This means that there will be a certain amount of freedom in choosing the various factorization and running coupling scales. For now, I shall take all of these scales to be the same, and refer to the common scale as Q^2. In addition, the uncertainties associated with different choices for the distribution functions, the QCD scale parameter Λ, and parton k_T smearing must all be examined. It would, of course, be possible to perform a systematic study of these uncertainties using just the data for direct-photon production. However, the basic formalism applies equally well to hadron and jet production, for which data are available over a similar kinematic range. By using data on all three types of processes we shall be able to explore more thoroughly the basic predictions of the formalism developed in Sec. II. The main goal of this section is to demonstrate the strengths and weaknesses of the leading-logarithm approximation as applied to large-transverse-momentum processes. With this as background the reader will be better able to appreciate some of the subtleties associated with the next-to-leading-order calculations.

Many authors have published leading-logarithm calculations for the types of observables to be discussed in this section. Indeed, one style of review would be to simply collect a representative sampling of such calculations and present them together. However, such an approach does not allow for the careful investigation of the various factors discussed in Sec. II. Therefore I have elected to perform all of the leading-logarithm calculations discussed in this section. This approach will allow me to discuss separately the uncertainties associated with the parton distributions, scale choices, etc. Similar work by other authors will be discussed at the relevant points in the text.

The Appendix contains expressions for the various observables that will be used in this review. Perhaps the simplest is the cross section for di-jet production [see Eqs.

(A7) and (A9)]. If one considers only 2→2 hard scattering in the leading-logarithm approximation and uses collinear kinematics, then measuring the momenta of both jets completely determines the parton-level kinematics. Data are available from the UA-2 Collaboration (Appel *et al.*, 1985) at $\sqrt{s}=546$ and 630 GeV for di-jet masses above 30 GeV. This corresponds roughly to p_T's being above 15 GeV, since the data have been presented with both jets having $|\eta| < 0.85$, where η is the jet's pseudorapidity. In Fig. 7 predictions are shown for the jet mass distributions at both energies, along with the data of the UA-2 Collaboration. Integrations over the above pseudorapidity range have been performed. The solid and dashed curves correspond to Set 1 ($\Lambda=0.2$ GeV/c) and Set 2 ($\Lambda=0.4$ GeV/c) structure functions, respectively. The choice $Q^2=2p_T^2$ has been used. The two sets of parton distributions yield very similar predictions over the mass range shown. As was discussed in Sec. II.B, the evolution of the distribution functions drives the two sets to very similar shapes at high values of Q^2. For this kinematic range there is, therefore, little reason to prefer one set over the other. Data have also been presented by the AFS Collaboration (Åkesson *et al.*, 1986a) at $\sqrt{s}=63$ GeV. These are compared with Sets 1 and 2 predictions in Fig. 8. Again, with $Q^2=2p_T^2$, the theoretical curves describe the data rather well. Notice that the difference between the two curves is somewhat larger here due to the lower values of Q^2. This trend continues as the energy is lowered further. Predictions using the same choices as discussed above are compared in Fig. 9 with
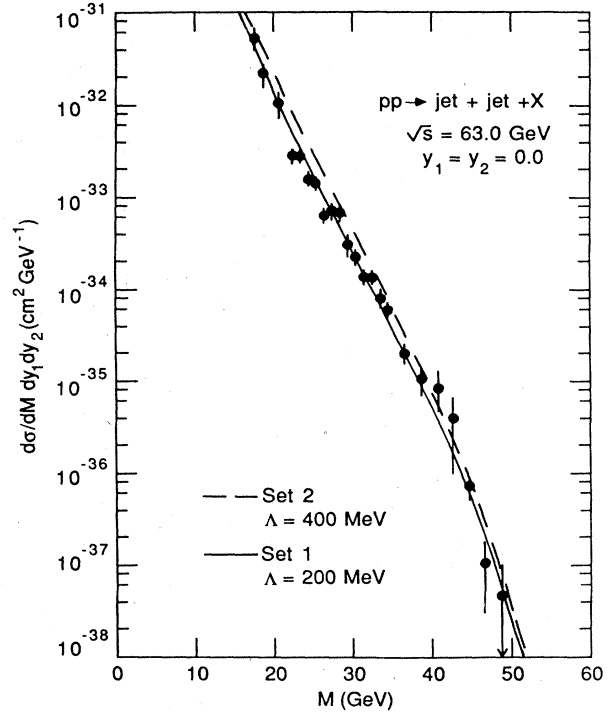
FIG. 8. Comparison between the di-jet data from the AFS Collaboration (Åkesson *et al.*, 1986a) and the leading-logarithm predictions discussed in the text.
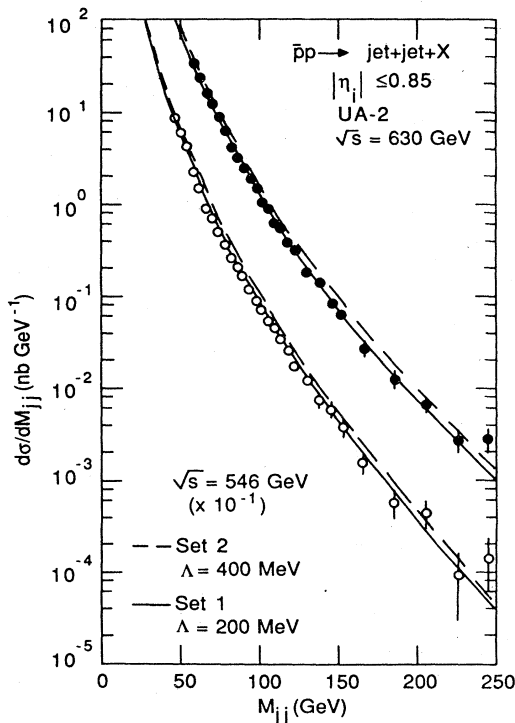

FIG. 7. Comparison between the di-jet data from the UA-2 Collaboration (Appel *et al.*, 1985) and the leading-logarithm predictions discussed in the text.
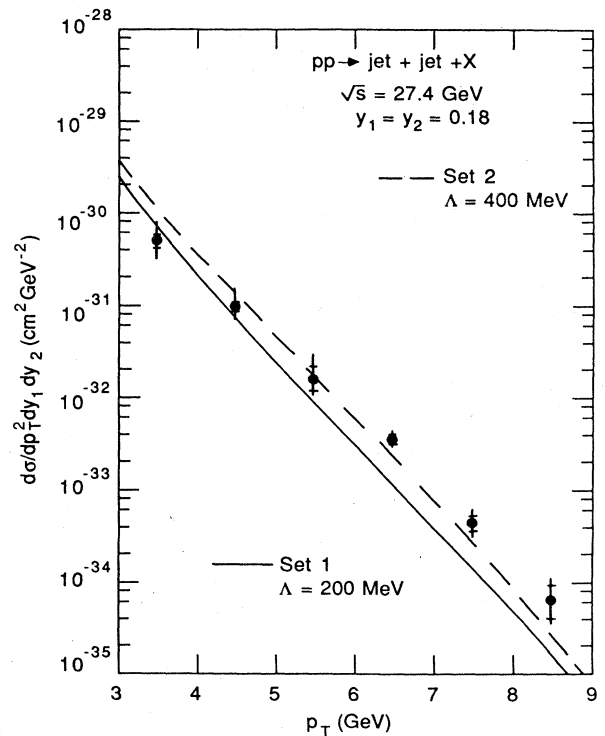

FIG. 9. Comparison between the di-jet data from E-609 (Arenton *et al.*, 1985) and the leading-logarithm predictions discussed in the text.

di-jet data at $\sqrt{s} = 27.4$ GeV from experiment E-609 at Fermilab (Arenton *et al.*, 1985). Again the spread between the two curves has increased. However, the theoretical band is in reasonable agreement with the data, especially if ones takes into account the 7% uncertainty in the transverse-momentum scale. Incidentally, note that the three data sets shown in Figs. 7—9 are all presented for slightly different observables. Therefore the data sets cannot be directly compared with each other. In particular, it is not possible to see if they satisfy a scaling law of the form shown in Eq. (9). Nevertheless, the differences between the different observables have been taken into account in the theoretical calculations, and the agreement between the predictions and the data shows that the observed energy dependence is in agreement with the theoretical expectations.

Next, consider the single-jet cross section [see Eq. (A3)]. New results from the UA-1 Collaboration (Arnison *et al.*, 1986a) and the UA-2 Collaboration (Appel *et al.*, 1985) are shown in Fig. 10 together with theoretical predictions made with the Set 1 distributions and $Q^2 = p_T^2$ (solid curve), $p_T^2/4$ (upper dashed curve), and $4p_T^2$ (lower dashed curve). This observable involves a single integration over one of the parton momentum fractions, which tends to further decrease the differences between predictions from Sets 1 and 2 distributions—for this case

they are barely distinguishable. The variation due to different definitions of Q^2 is larger than that due to the distribution choice and, for clarity, only the Set 1 predictions are shown.

The variation in the cross section shown in Fig. 10 due to the different Q^2 definitions amounts to about a factor of 3 across the entire p_T range shown. This variation is larger than that which would result from choosing a single scale and introducing "K factors" as calculated using the soft-gluon approximation. As mentioned in Sec. II.E, such K factors do not contain the next-to-leading terms that partially compensate for changes in the Q^2 definition. Thus one does not know *a priori* which of the choices should be used when the K factors are included. To put this another way, any set of predictions obtained using the K factors can be duplicated without them, but with another choice made for the definition of Q^2. This ambiguity is a feature of the leading-logarithm approximation that must be understood and allowed for.

Predictions for the single-jet cross section at lower energies are compared with available data in Fig. 11. All three data sets have been analyzed in the same way, using similar jet definitions. This is an important point, especially at the lower energies where the jet signals are relatively harder to separate from the minimum-bias background. The three curves at each energy correspond to
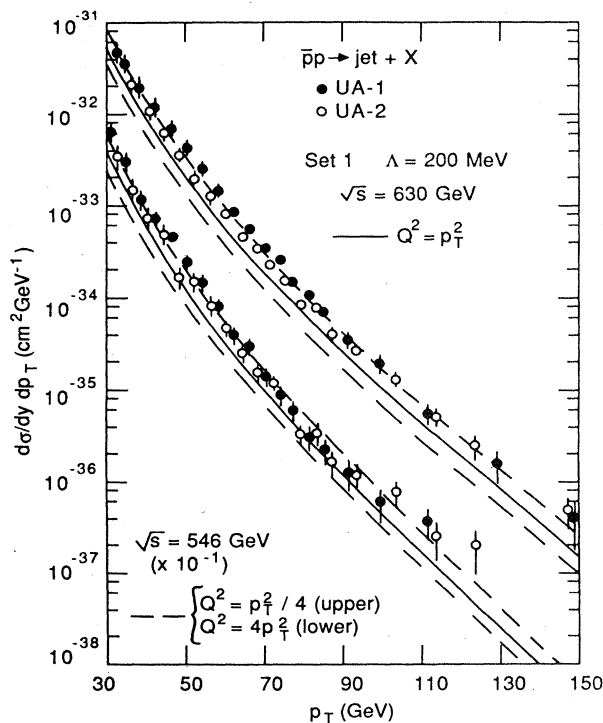

FIG. 10. Comparison between data for the inclusive single-jet cross section and several leading-logarithm predictions corresponding to different choices for Q^2. ●, UA-1 Collaboration (Arnison *et al.*, 1986a); ○, UA-2 Collaboration (Appel *et al.*, 1985). For clarity, only a portion of each data set has been shown.
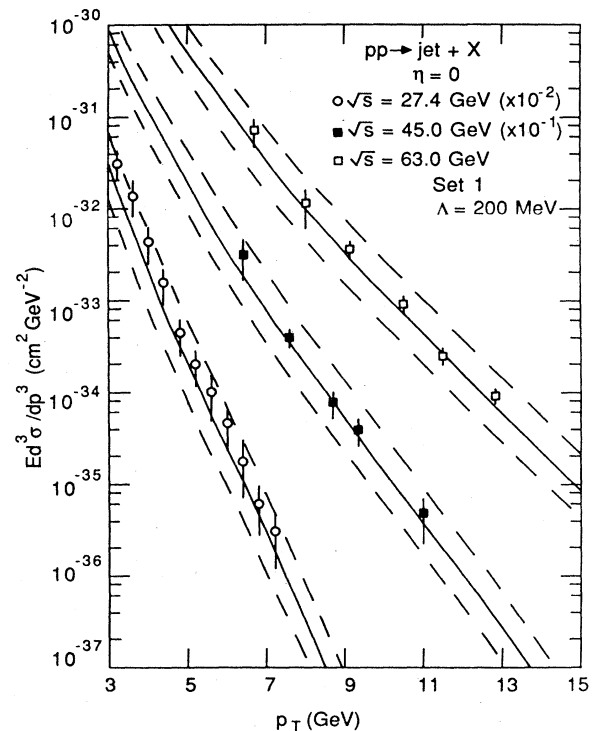
FIG. 11. Comparison between data for the inclusive single-jet invariant cross section and several leading-logarithm predictions. The notation is the same as for Fig. 10. □ and ■, AFS Collaboration (Åkesson *et al.*, 1983); ○, E-609 (Cormell *et al.*, 1985).

the same scale choices as for Fig. 10. Notice that the spread between the two dashed curves varies between a factor of 5 to 6 in this energy range, whereas it was about a factor of 3 for the higher energies shown in Fig. 10. This again reflects the more rapid variation of the logarithms at the lower values of Q^2.

From the results shown in Figs. 7—11 and the discussion above, it should be clear that the overall normalization of a particular process is not predicted with great accuracy in the leading-logarithm approximation. The sensitivity to the choices made for the factorization scale, and for the argument of the running coupling, can lead to relatively large variations between otherwise identical calculations. On the other hand, on the optimistic side, the scale change by a factor of 16 shown in Figs. 10 and 11 results in a somewhat smaller change in the cross sections. More to the point, however, is the fact that the energy dependence of the various observables is predictable in that it depends only slightly on the choices of scale.

In order to pursue this last point, I have plotted the ratio of the jet cross sections from both the UA-1 and UA-2 Collaborations at $\sqrt{s} = 546$ and 630 GeV in Fig. 12. Shown also is the prediction for $Q^2 = p_T^2$. For comparison, the curves for $Q^2 = 4p_T^2$ and $p_T^2/4$ lie within a few percent above and below the solid curve, respectively. The differences are too small to be shown accurately on this scale. This is an example of a prediction that has virtually no dependence upon the factorization scale or the choice of the parton distributions. Rather, the energy dependence follows from dimensional arguments with some modest logarithmic corrections from the running coupling and from scaling violations in the distribution functions.

The preceding point can be investigated further by extracting the power-law behavior of the data at fixed values of x_T and θ, as discussed in Sec. II.D [see Eq. (9)]. For example, the data of the AFS Collaboration (Åkesson

et al., 1983) yield $n = 5.3 \pm 0.2$ for $\sqrt{s}$ between 45 and 63 GeV. The UA-2 Collaboration (Appel et al., 1985) finds $n = 4.5 \pm 0.3$ for $\sqrt{s}$ between 546 and 630 GeV. On the other hand, a global fit to both data sets yields $n = 4.74 \pm 0.06$. The decrease of n with increasing values of s is indicative of a violation of the scaling prediction contained in Eq. (9). This is a manifestation of the logarithmic Q^2 dependence referred to above. For comparison, recall that the parton model scaling prediction is $n = 4$, so that the deviations from exact scaling in this kinematic region are not large, and they decrease as the energy increases. This latter point is easily understood: as the arguments of the logarithms keep increasing, the rate of change of the logarithm terms becomes ever smaller.

Another interesting point is raised when we compare the results for the di-jet calculations in Figs. 7—9 and those for the single-jet cross sections in Figs. 10 and 11. For the di-jet case, a good description was obtained with $Q^2 = 2p_T^2$. On the other hand, the single-jet data seem to be best described by a somewhat smaller choice. The curves in Figs. 10 and 11 suggest that an appropriate choice would be $Q^2 = p_T^2/2$. It is possible that this difference may simply be attributable to the rather large systematic errors inherent in the calorimetric measurement of jet cross sections (45% for the UA-2 Collaboration and 70% for the UA-1 Collaboration, for example). On the other hand, it must be remembered that the next-to-leading-order corrections to the leading-logarithm approximation will be different for the single-jet and di-jet cross sections. It would therefore be interesting to see if both cross sections could be described with a common set of choices for the various scales. Notice that the soft-gluon approach would predict the same form for the higher-order corrections for the two types of cross sections and therefore would not account for the difference.

A final comment is in order concerning the comparison with jet cross sections. I have simply identified the outgoing parton four-vectors as being identical with those of the outgoing jets. Nowhere in the leading-logarithm approximation is there any allowance made for variations in the experimental definition of a jet. In order to see such a variation, the next-to-leading logarithms must be included. It is thus rather remarkable, as well as encouraging, to see the good agreement between the theory and data shown in Figs. 7—12. There is clearly room for more theoretical work, however, because the next-to-leading-logarithm calculations should help to reduce the level of uncertainty associated with the overall normalization of the theoretical curves.

Next consider the predictions for single-particle invariant cross sections [see Eqs. (A4) and (A5)]. Figure 13 shows a comparison between the theoretical predictions and π^0 data at $\sqrt{s} = 540$ GeV from the UA-2 Collaboration (Banner et al., 1985). The two photons from the π^0 decay have not been resolved for these data. Therefore the data actually correspond to a combination of π^0, direct-photon, and η contributions. The theoretical curves were obtained by adding the results for both π^0
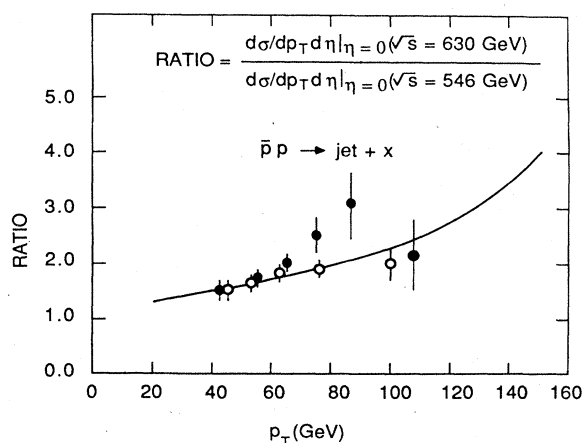

FIG. 12. Comparison between theory and experiment for the ratio of the inclusive single-jet cross sections at $\sqrt{s} = 546$ and 630 GeV: ●, UA-1 Collaboration (Arnison et al., 1986a); ○, UA-2 Collaboration (Appel et al., 1985).

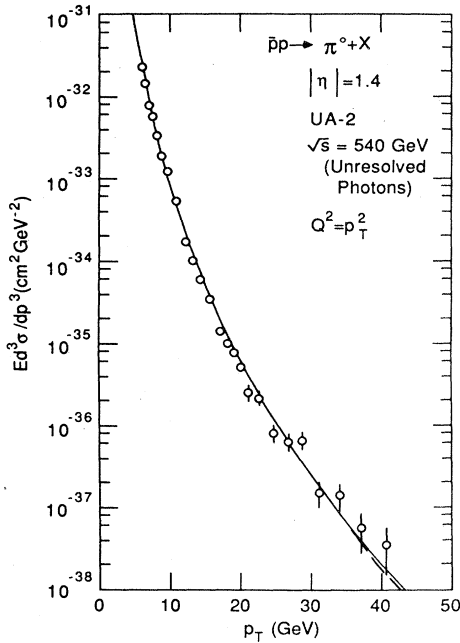FIG. 13. Comparison between data for inclusive π^0 production (Banner *et al.*, 1985) and the leading-logarithm predictions discussed in the text.

and single-photon production. (Including an η contribution could increase the predictions by about 20% of the π^0 signal.) Again, Sets 1 and 2 predictions are shown by solid and dashed curves, and in this case they are nearly indistinguishable over almost the entire p_T range shown.

In Fig. 14 a similar comparison is made using data for charged-pion production (Breakstone *et al.*, (1984). The dotted curve shows the effect of including k_T smearing with $\langle k_T^2 \rangle = 0.90$ GeV^2 with the Set 2 distributions. This value of $\langle k_T^2 \rangle$ corresponds to $\langle k_T \rangle = 0.84$ GeV, since a Gaussian distribution has been assumed. This large value is used simply to demonstrate typical effects of applying the k_T-smearing formalism of Sec. II.D. Other values can certainly be used, as the whole procedure is just a model, after all. Applying k_T smearing with the Set 1 distributions raises the solid curve approximately to the dashed one and, for clarify, the result has not been shown. The same features are examined further in Fig. 15, in which, a comparison with π^0 data (Kourkoumelis *et al.*, 1980) is shown. The data in Fig. 15 correspond to pions in which both of the decay γ's have been resolved. Therefore no direct-photon component has been included in the theoretical curves. From the results shown in both Figs. 14 and 15, one can clearly see that the k_T-smearing effects are more significant for the steeper, low-energy predictions.

The curves in Figs. 13–15 have been obtained using $Q^2 = p_T^2$, where p_T is that of the hadron. Due to the fragmentation process, this is somewhat less than the transverse momentum of the parent parton (or jet). Curves corresponding to other choices for Q^2 have not been
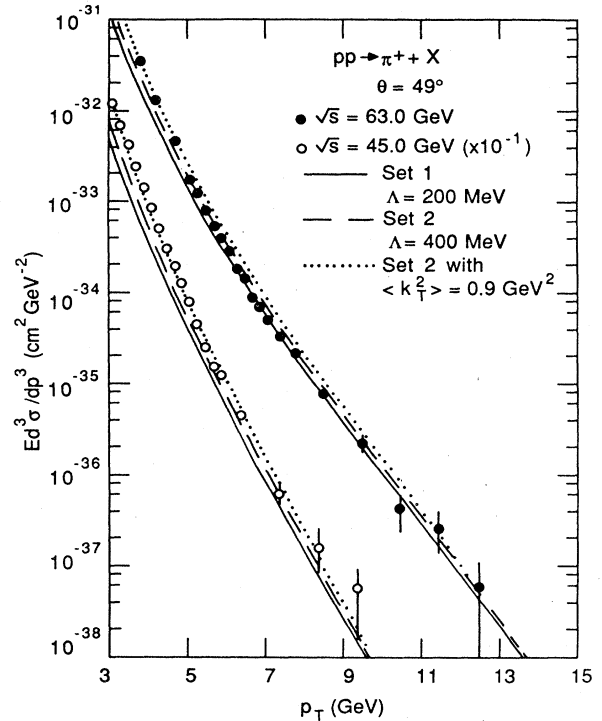

FIG. 14. Comparison between data for inclusive π^+ production (Breakstone *et al.*, 1984) and the leading-logarithm predictions discussed in the text.
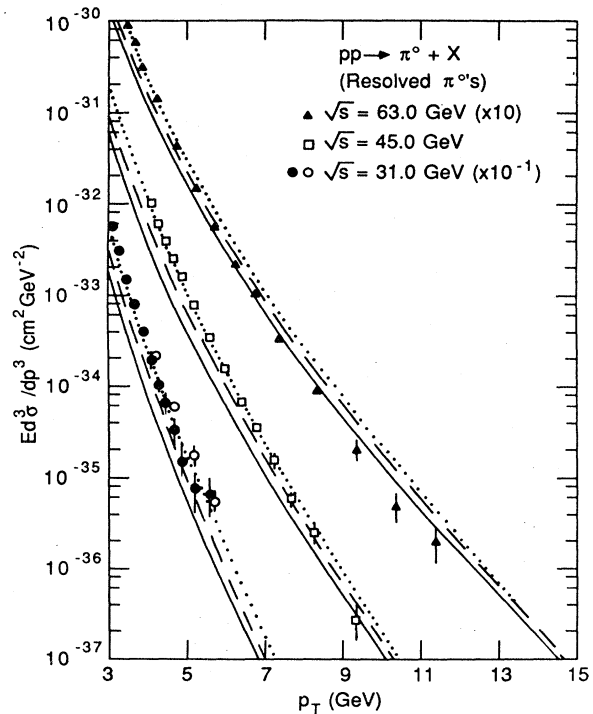

FIG. 15. Comparison between data for inclusive π^0 production (Kourkoumelis *et al.*, 1980) and the leading-logarithm predictions discussed in the text. The notation is the same as for Fig. 14.

shown, but there is clearly the same degree of flexibility here as was shown for the jet cross sections. Further fine tuning of the predictions would be of little benefit, at this time. The major point to be made here is that the energy dependence is correctly described from $\sqrt{s} = 540$ GeV down to energies in the ISR range, for p_T above about 7 GeV. Notice, however, that at lower p_T values there is a tendency for the theory to fall systematically below the data as the energy is reduced. The addition of k_T smearing raises the curves somewhat, providing a better description of the data. However, as discussed in Sec. II, the smearing procedure is model dependent. This subject will be discussed in more detail with regard to the comparison with the direct-photon data.

Incidentally, one might wonder why k_T effects were not necessary for the description of the jet data in Fig. 11. In part this is due simply to the larger errors on the data. In addition, there is the fact that k_T effects are somewhat less important for jet production than for hadron production at the same values of p_T and $\sqrt{s}$. This is due to the somewhat flatter p_T dependence of the jet cross section. Although not shown, k_T smearing of the magnitude used above would increase the predictions for $\sqrt{s} = 27.4$ GeV by about a factor of 2 at $p_T = 3$ GeV, with the size of the effect smoothly decreasing with increasing p_T. The effect at fixed p_T is smaller at the higher energies.

As mentioned in the discussion of k_T smearing in Sec. II, the enhancement is due to having a single-arm trigger that will preferentially select those events in which the parton-parton center-of-mass frame possesses some transverse momentum toward the trigger. This effect can be nearly eliminated, however, if one uses a double-arm trigger, since then there is no preference for any transverse motion of the parton-parton system. A detailed discussion of k_T smearing and double-arm triggers can be found in the paper of Baier, Engels, and Petersson (1979). The CCOR Collaboration (Angelis et al., 1982) has measured the $\pi^0 \pi^0$ cross section using a double-arm trigger. With the π^0's on opposite sides of the event, the k_T-smearing effects are minimized. The CCOR data for the di-pion mass distribution have been presented with a series of cuts on the di-pion rapidity ($|Y| < 0.35$), on the p_T imbalance between the two pions (< 1 GeV), and on the parton-parton center-of-mass scattering angle ($\cos\theta^* < 0.4$). In order to enforce these cuts in the presence of parton k_T effects it is necessary to use a Monte Carlo simulation. Such a program has been written and a comparison between calculations with or without the k_T effects included shows essentially no difference, within the statistics of the Monte Carlo simulation. It is therefore possible to ignore the k_T effects for this observable and to use the simplification of collinear kinematics, thus obtaining a simple expression for the di-pion mass distribution, into which it is easy to incorporate the effects of the CCOR cuts. This is discussed in detail in the Appendix.

The CCOR di-pion data are shown in Fig. 16, along with the theoretical results from the Set 1 distributions. In this experiment the π^0 decay photons were not
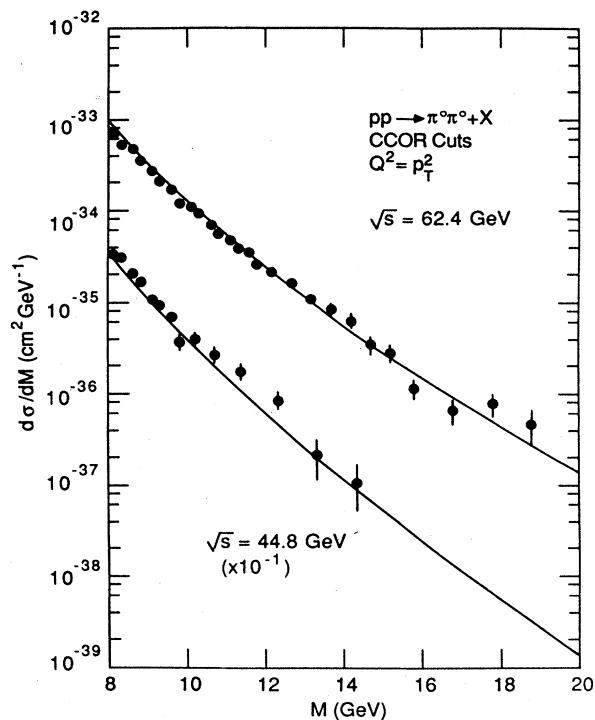

FIG. 16. Comparison between data for neutral di-pion production (Angelis et al., 1982) and the leading-logarithm predictions discussed in the text.

resolved, so a direct-photon contribution has been included in the theoretical curves. The good agreement shown in Fig. 16 serves to illustrate the utility of a double-arm trigger in removing the need for introducing model-dependent k_T-smearing effects. However, it must be mentioned that the overall normalization depends even more strongly on the Q^2 choice than in the case of jets. This results from having two fragmentation functions in the final state, both of which have scaling violations.

The main points of this introductory subsection can be summarized as follows.

(1) The energy and p_T dependence of single-jet and di-jet data can be described well using the leading-logarithm formalism.

(2) The overall normalization of the various jet cross sections is consistent with the range obtained within the leading-logarithm approximation.

(3) The single-particle data are also described well in the high-p_T region. If one includes model-dependent parton k_T effects, the region of agreement can be extended to lower p_T and $\sqrt{s}$ values.

(4) The parton k_T effects increase in importance as the cross section becomes steeper in p_T. They are thus most important for the single-particle predictions and less so for jets and direct photons.

(5) The effects of parton transverse momentum can be reduced by considering observables with two hadrons or jets in which the transverse momenta are constrained to be approximately balanced.

In this subsection I have dealt exclusively with data for high-p_T cross sections. More data are available for different observables, such as two-particle correlations, away-side p_T distributions, etc. It would go beyond the scope of this review to include a comprehensive summary of all of these data. Rather, my goal here has been to illustrate the features and limitations of the leading-logarithm approximation as used in the description of high-p_T jet and single-particle cross sections, in preparation for a more detailed discussion of the direct-photon data. It is to this subject that I now turn.

B. Direct-photon cross sections

The relative simplicity of direct-photon production was recognized at an early stage in the development of high-p_T phenomenology (Farrar, 1977). Accordingly there were many suggestions for methods of testing QCD using high-p_T photon-triggered data. Some early studies include those of Soh, Pac, Lee, and Choi (1978), Halzen and Scott (1978a, 1978b, 1980a, 1980b), Benary, Gotsman, and Lissauer (1981), and Contogouris, Papadopoulos, and Hongoh (1979). The importance of studying the correlations between the trigger photon and associated hadrons or jets was also pointed out by many authors. Some of the early references include the papers of Cormell and Owens (1980), Baier, Engels, and Petersson (1980), Contogouris, Papadopoulos, and Papavassiliou (1981), and Dechantsreiter, Halzen, and Scott (1981). Additional discussion of the earlier theoretical and experimental work may be found in the review by Ferbel and Molzen (1984). Some of the more recent experimental results are reviewed by Rutherfoord (1985), Treille (1985), and Ferbel (1986).

As in the previous discussions of jet and single-particle data, I shall begin the comparison between theory and experiment using data at the highest available energy. The UA-2 Collaboration has reported data for direct-photon production in $\bar{p}p$ collisions at $\sqrt{s} = 630$ GeV (Appel et al., 1986). In this work a background subtraction was made to remove meson-induced signals. Corrections were included to account for various cuts made as part of the event selection. However, it should be noted that an isolation cut on the photon candidates was used in order to reduce the π^0 and η backgrounds, and this partially suppressed the bremsstrahlung contribution. In Fig. 17 the data at $\eta = 0$ are compared with predictions obtained with the Set 1 distributions. The Q^2 definition was taken as $p_T^2/2$, following the comparison with the single-jet data. The full leading-logarithm calculation is shown by the solid curve, whereas the dotted curve shows the effect of excluding the bremsstrahlung contribution. This latter curve is included in order to give a feeling for the possible effects of the photon isolation cut. The agreement with the data appears to be satisfactory. The Set 2 distributions can also be employed and, with a suitable change in the Q^2 definition, they yield similar predictions. It is worth noting that the bremsstrahlung contribution is about 30% of the total shown by the solid curve in Fig.
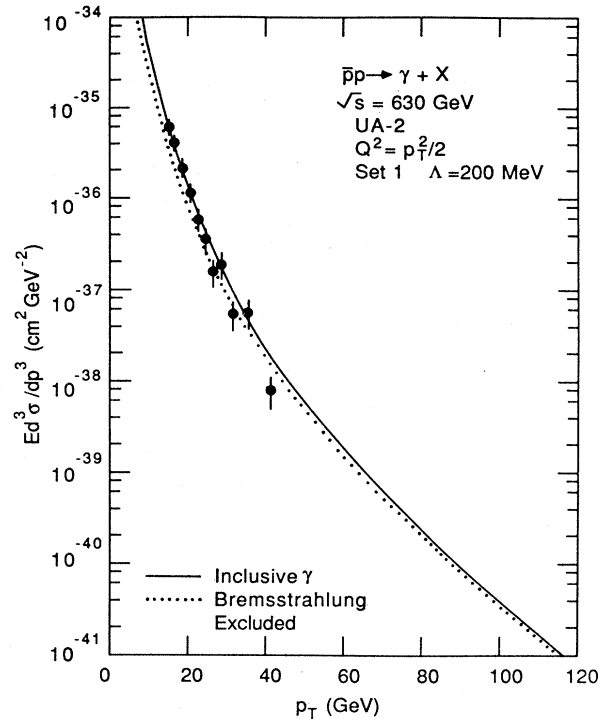

FIG. 17. Comparison between data for direct-photon production at $\eta = 0$ from the UA-2 Collaboration (Appel et al., 1986) and the leading-logarithm predictions discussed in the text.

17 in the region where there are data. This is shown more clearly in Fig. 27 below and is discussed in detail later in this section. If only the inclusive cross section is being considered, the question of whether or not to include the bremsstrahlung component is not too significant, since the overall normalization can easily be shifted by a similar amount, as has been discussed previously. However, the nature of the bremsstrahlung contribution does become important when questions regarding correlations are considered, as will be discussed later.

In the same reference, the UA-2 Collaboration also presented data on the photon and π^0 cross sections at $\eta = 1.4$, with the photon contribution to the π^0 cross section already subtracted. In Fig. 18 these data are compared to the Set 1 predictions. For consistency with the previous single-particle calculation, $Q^2 = p_T^2$ was used. Using $Q^2 = p_T^2/2$ for the π^0 calculation, as was done for the case of direct-photon production, would increase the prediction by about 50%.

Data for pp interactions have been obtained at the ISR by several groups. At $\sqrt{s} = 63$ GeV, the CCOR Collaboration has presented their results in the paper of Angelis et al. (1980). These data were obtained with an isolation cut on the photon candidates. The resulting cross section must be corrected for this cut in order to obtain a fully inclusive cross section. A multiplicative factor of 0.8 is quoted for this correction. The inclusive cross-section data, including the factor of 0.8, are shown in Fig. 19 by the solid triangles.
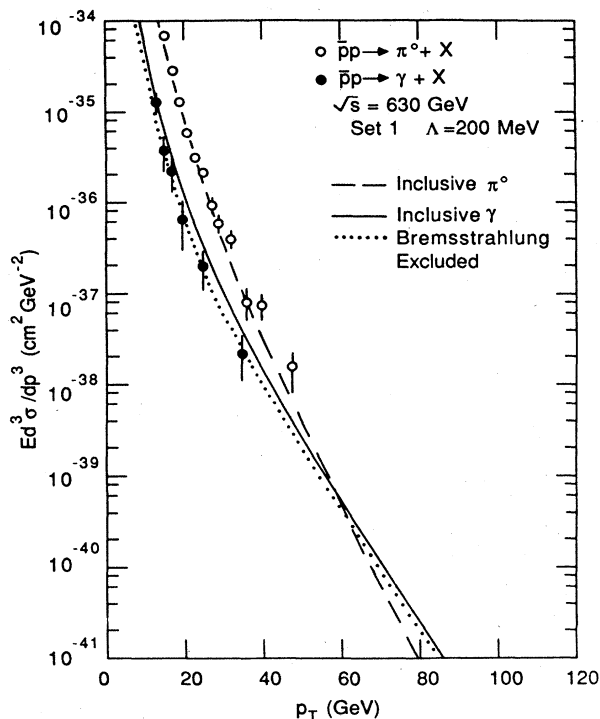
FIG. 18. Comparison between the leading-logarithm predictions discussed in the text and data for both direct-photon and π^0 production at $\eta = 1.4$ from Appel *et al.* (1986).
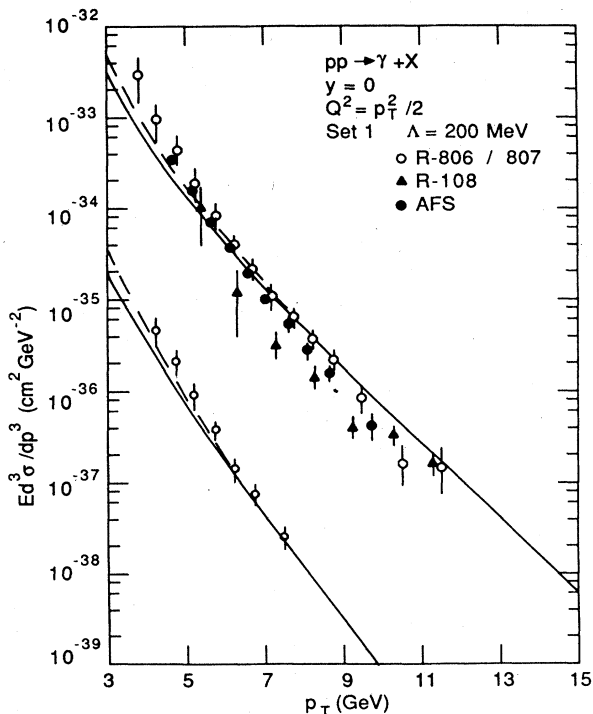

FIG. 19. Comparison between inclusive direct-photon-production data and the leading-logarithm predictions discussed in the text; O at 62 GeV, Anassontzis *et al.*, 1982; O at 45 GeV, Burkert, 1983; △, Angelis *et al.*, 1980; ●, Åkesson *et al.*, 1985.

Additional data at $\sqrt{s} = 63$ GeV have been presented by Anassontzis *et al.* (1982). These data have been fully corrected for the effects of the photon isolation cut and correspond to a fully inclusive measurement. Inclusive cross-section data from the same group at $\sqrt{s} = 45$ GeV are presented in the paper of Burkert (1983). Both data sets are shown in Fig. 19 by the open circles. The errors shown include both statistical and systematic uncertainties.

Preliminary data from the AFS Collaboration at $\sqrt{s} = 63$ GeV (Åkesson *et al.*, 1985) are shown in Fig. 19 by the solid circles. Only the statistical errors are shown; there is an additional overall 24% systematic uncertainty.

There is broad agreement among the various data sets shown in Fig. 19, once the systematic errors are taken into account. The comparison between the older data sets is discussed in some detail by Ferbel and Molzon (1984). Predictions obtained with the Set 1 distributions with $Q^2 = p_T^2/2$ are shown by the solid curves in Fig. 19. There is reasonable agreement with the data at the upper end of the p_T range, but there is a systematic tendency to underestimate the data for p_T below about 6 GeV. This is similar to the situation for single-pion production. The effect of including parton k_T smearing with $\langle k_T^2 \rangle = 0.9$ GeV^2 is shown by the dashed curves. The increase is about a factor of 1.6 at $p_T = 3$ GeV, and the two calculations merge smoothly as p_T increases.

Two experiments, NA-24 and NA-3, have obtained data with π^+, π^-, and proton beams at $\sqrt{s} = 23.7$ and 19.4 GeV, respectively. The NA-24 data have $y \approx 0$ and were obtained with a hydrogen target. The preliminary data from DeMarzo *et al.* (1985) are shown in Fig. 20. Again, the solid curves were obtained with the Set 1 distributions and $Q^2 = p_T^2/2$. The dashed curves show the effect of including k_T smearing, as discussed in Sec. II. Notice that the increase of the cross section is largest for the steeper proton cross section. At $p_T = 3$ GeV the increase is about a factor of 2, illustrating the greater importance of the smearing for lower energies.

The data from the NA-3 experiment (Badier *et al.*, 1986) are shown in Fig. 21. These were obtained with a carbon target, and I have rescaled them assuming an A^1 dependence. The open and closed symbols correspond to two different triggers, and are for slightly different rapidity intervals. The curves were calculated by averaging the invariant cross section over the range $-0.4 \le y \le 1.0$, which corresponds to the average of the two regions covered by the different triggers. It is important to perform the averaging, because there is a significant rapidity dependence over this broad interval. The effect becomes rather pronounced at the high end of the available p_T range. At this low value of $\sqrt{s}$, the leading-logarithm predictions shown by the solid curves are definitely below the data over the entire measured p_T range. The model-dependent k_T smearing is able to bring the predictions upward in approximate agreement with the data. Notice that the effect of the smearing has increased again with a lowering of the energy. Also shown in Fig. 21 is the result of changing to the Set 2 parton distributions for the
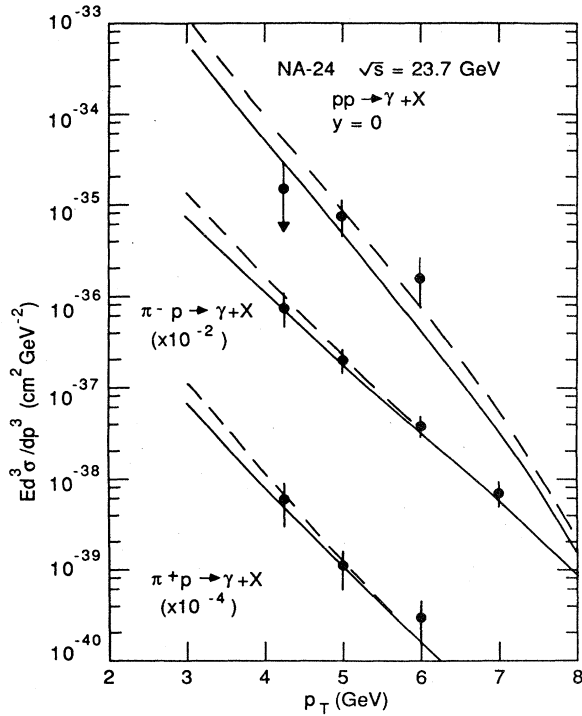
FIG. 20. Comparison between the leading-logarithm predictions with (dashed curves) and without (solid curves) k_T smearing and data for inclusive photon production from the NA-24 experiment (DeMarzo *et al.*, 1985).
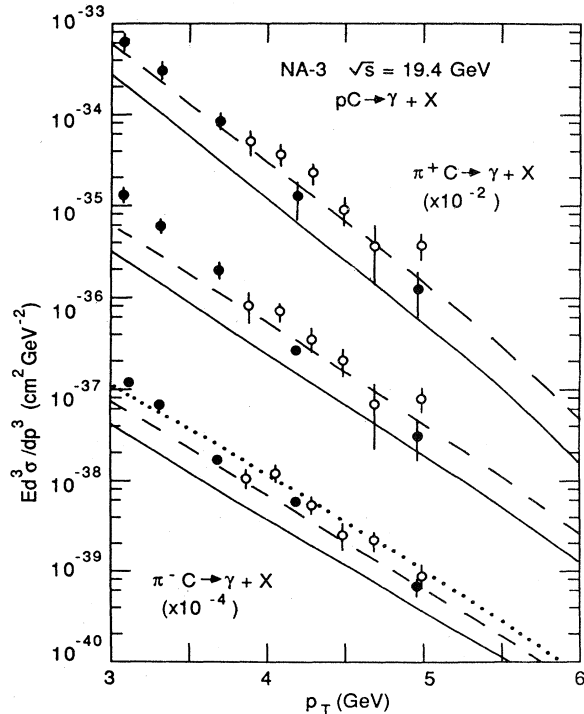

FIG. 21. Comparison between the leading-logarithm predictions discussed in the text and data for inclusive photon production from the NA-3 experiment (Badier *et al.*, 1985) with proton (upper), π^+ (middle), and π^- (lower) beams.

π^- case. The dotted curve is somewhat higher than the dashed one, in part because of the harder pion and nucleon-gluon distributions in Set 2, and also as a result of the larger value of Λ used with Set 2.

Figures 22 and 23 show the ratio of the π^-— and π^+—induced direct-photon cross sections from the NA-24 and NA-3 experiments, respectively. The Set 1 predictions are shown by the solid curves, and the dotted curve in Fig. 22 corresponds to the Set 2 distributions. This cross-section ratio is insensitive to the k_T smearing because of the ratio's slow growth with p_T.

In the absence of photon bremsstrahlung contributions there are only two hard-scattering subprocesses for producing direct photons. These are the Compton subprocesses $gq \rightarrow \gamma q$, illustrated in Fig. 2(a), and the annihilation subprocess $q\bar{q} \rightarrow \gamma g$, shown in Fig. 2(b). If only the Compton term contributed, the ratio of the π^- and π^+ cross sections would be constant at one. However, the presence of a $\bar{u}$ quark in the π^-, as opposed to a d in the π^+, means that the annihilation subprocess will make a relatively larger contribution in the π^- case. This follows both from the larger charge for the $\bar{u}$ quark and from the fact that the u-quark distribution in a proton is larger than that of the d quark. At low p_T the gluon distributions are important, so that the Compton process dominates and the ratio is near unity, as shown in both Figs. 22 and 23. As the transverse momentum increases, the annihilation process makes an increasingly important contribution and the ratio rises. The predictions shown in the figures are compatible with the existing data. In particular, notice the relatively small difference between the predictions of the two sets of distributions. The effect of the harder Set 2 gluons is washed out by the integrations performed to calculate the single-photon invariant cross section. A double-arm measurement, in which the kinematics can be more tightly constrained, would be more sensitive to different gluon shapes. This will be discussed in detail in the next subsection.

The preceding results show that it is possible to describe the single-photon invariant cross section adequately within the context of the leading-logarithm ap-
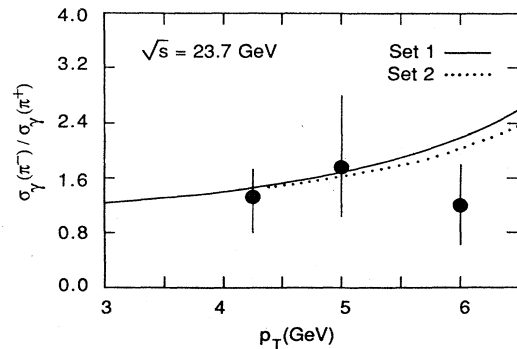

FIG. 22. Comparison between theory and experiment for the ratio of direct-photon production from π^- and π^+ beams. The data are from the NA-24 experiment (DeMarzo *et al.*, 1985).
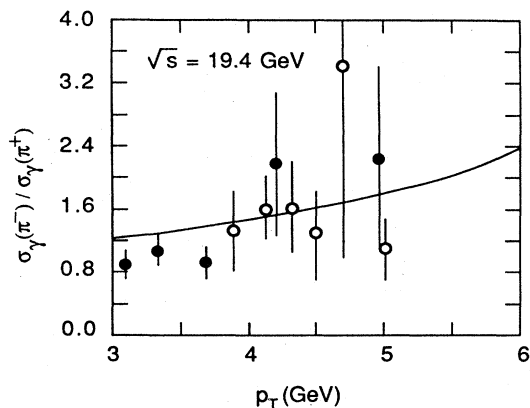
FIG. 23. Comparison between theory and experiment for the ratio of direct-photon production from π^- and π^+ beams. The data are from the NA-3 experiment (Badier et al., 1986).

proximation, suitably augmented by the model-dependent k_T smearing. However, the prescription for the predictions presented here is not unique. For example, a description of similar quality has been presented by Argyres, Contogouris, Sanielevici, and Tanaka (1984), Contogouris, Mebarki, Tanaka, and Vlassopulos (1985), and Contogouris, Mebarki, and Tanaka (1986). These calculations all utilize the leading-logarithm approximation, k_T smearing with a somewhat smaller value for $\langle k_T^2 \rangle$, and K factors calculated in the soft-gluon approximation. The increase from the K factors is compensated in part by choosing $Q^2 = p_T^2$. The results are quite similar to those shown here. While this flexibility may be viewed as a weakness of the leading-logarithm approximation, one can still conclude that the general features of the data are in accordance with the theoretical expectations. What is needed is a way to remove some of the flexibility associated with the theoretical calculations.

The crucial ingredient needed to improve the precision of the theoretical predictions is a complete next-to-leading-logarithm calculation. A calculation based on all $O(\alpha\alpha_s^2)$ subprocesses in which the photon participates directly in the hard scattering has been performed (Aurenche, Douri, Baier, Fontannaz, and Schiff, 1984). Some of the relevant Feynman graphs have already been shown in Fig. 2. As was discussed previously in Sec. II.E, the presence of the next-to-leading logarithms helps to stabilize the theoretical predictions, by making them less sensitive to variations in the definitions of the factorization scales and the argument of the running coupling. Of course, if the exact calculation were performed to all orders of perturbation theory, then the result would not depend on the particular choices made; however, with an approximate calculation some dependence on the choice of scales will remain. This opens up the question of how to make the optimal choice of scales for a particular calculation. Various schemes for selecting the optimal scales have been reviewed by Duke and Roberts (1985). For the case of direct-photon production, this problem is under study by the Bielefeld/LAPP/Orsay group (Aurenche,

Baier, Fontannaz, and Schiff, 1986b). Using their next-to-leading-order results they have sought to determine the optimal factorization and running coupling scales with the PMS criterion (Stevenson, 1981a, 1981b; Politzer, 1982). The basic idea is to vary both the coupling (α_s) and the factorization scale (M_d^2) until a stationary point for the cross section is found. This point then represents the optimal perturbative result to a given order. The fragmentation scale (M_f^2) is not varied since, as discussed above, the bremsstrahlung component does not make a large contribution in the high-p_T region. The optimization procedure must be carried out at each point in phase space. A sample result is shown in Fig. 24 (Aurenche, Baier, Fontannaz, and Schiff, 1986b). The factorization scale for the distribution functions is parametrized as $M_d^2 = C_M p_T^2$, and the results are shown as a contour plot of the invariant cross section in units of 10^{-37} cm^2/GeV^2 at $p_T = 10$ GeV and $\sqrt{s} = 63$ GeV. The plot shows a saddle-point structure, with the stationary point corresponding roughly to $C_M = 0.2$. Note that, in the vicinity of the stationary point, the sensitivity to the factorization scale nearly vanishes. The dependence on the coupling near the stationary point is such that the optimized cross section is a maximum—varying α_s for fixed C_M causes a decrease of the cross section. This is in accordance with the parabolic dependence that results from an implementation of the PMS scheme. Given an optimal value for the coupling, it is possible to work backward and deduce what value one must choose for Q^2; this point has been discussed by Stevenson (1981a, 1981b). For the result shown in Fig. 24, the approximate value for Q^2 at $p_T = 10$ GeV is about 5 GeV^2 if α_s is evaluated with four flavors, $\Lambda_{\overline{MS}} = 200$ MeV, and the two-loop expression is used. Clearly, the optimal scale for Q^2 is much less than p_T^2. Although this work is still in progress, some preliminary
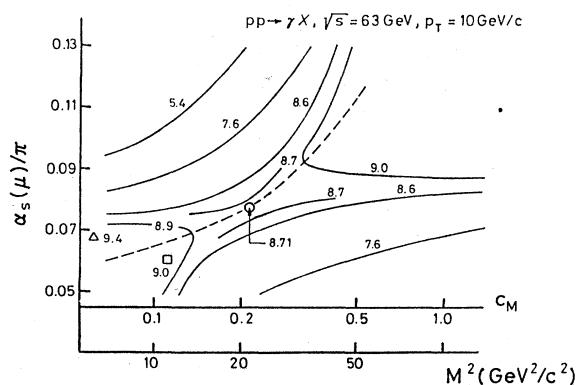

FIG. 24. Contour plot for direct-photon production in pp collisions from Aurenche, Baier, Fontannaz, and Schiff (1986b). The contours are for constant cross section at $p_T = 10$ GeV and $\sqrt{s} = 63$ GeV from a next-to-leading-logarithm calculation (Aurenche et al., 1986). The units are 0.1 pb/GeV^2: o, two-scale PMS result; Δ, one-scale PMS result; $\square$, FAC result. The contours form a saddle-point structure with the dashed curve showing the ridge line.

conclusions are available. First, the optimized cross section yields factorization scales that tend to be somewhat smaller than the "conventional" choices. Moreover, the argument of the running coupling tends to be much smaller than the factorization scale. In the region of p_T below about 10 GeV, this latter effect leads to a fairly rapid variation of the running coupling, which, in turn, results in a significant increase in the predictions at fixed-target energies, and a less dramatic effect at collider energies, when compared with the single-scale calculations used above. This point will be reexamined when we discuss correlations.

For comparison, two other optimization results are shown in Fig. 24. The triangle denotes the result if the factorization scale and the argument of the running coupling are fixed to be the same. This is the so-called "one-scale" PMS result. The square denotes the result of the method of fastest apparent convergence (FAC) (Grunberg, 1980, 1984). In this technique, the factorization scale and the argument of the running coupling are again taken to be the same and are varied until the next-order correction vanishes. Notice that all three results are within a few percent of each other.

Optimized predictions have been published in conjunction with NA-3 and NA-24 results. The predictions are in good agreement with the data from both groups. This is important, since there is very little flexibility remaining in these optimized predictions. For example, there appears to be no need for large k_T-smearing corrections. The $2\rightarrow3$ sub-processes contribute some of the smearing effect, but here the contribution is calculated without any model assumptions. There could, in principle, be a small "primordial k_T" contribution, but presumably the average value of k_T would be much less than that used in the model-dependent results discussed previously. As was mentioned in Sec. II.D, as additional QCD perturbative contributions are included, the need for phenomenological smearing corrections is decreased. Additional attractive features of the optimization procedure are that it provides specific choices for the various scales, and that the calculation is relatively stable with respect to small variations about the optimum point.

It may appear that the optimization procedure is rather complex in that the predictions at each point in phase space must be optimized separately. However, in practice it should be possible to parametrize the dependence of the various scales in a reasonably simple way and then fix the parameters by optimizing at a few points. In this way optimized predictions should be obtainable without too much more effort than usual. The reward for the extra effort is a decrease in the model dependency of the result. In this regard, it is worth noting that other schemes for fixing the various scales (such as the method of fastest apparent conversion, for example) have been found to yield results similar to those obtained with the PMS scheme. This is encouraging, since that means that the remaining model dependency is not large.

Summarizing this section, we have seen that the theoretical predictions for the direct-photon invariant cross section are in accordance with the data. The large degree of flexibility associated with the leading-logarithm calculations and the model-dependent k_T smearing can be reduced once the next-to-leading-logarithm corrections are included. It is now time to turn to other observables that can be of use in providing further tests of the theory.

C. Correlations

The subject of correlations in direct-photon production is interesting for several reasons. First, the simple structure that exists at the lowest order of perturbation theory makes several striking predictions for the correlations between the trigger photon and associated high-p_T hadrons. These predictions can be used to test the validity of the QCD description of the process of direct-photon production. Second, simultaneous measurement of the four-vectors of the trigger photon and the recoiling away-side jet (or even the leading away-side hadron) allows the underlying parton-level kinematics to be more tightly constrained than is the case for the single-photon invariant cross section. This, in turn, can be used to provide constraints on, or perhaps even measurements of, various parton distribution and fragmentation functions. The methods by which correlation measurements can be so employed is the subject of this section.

1. Toward-side hadrons

First, consider correlations between the trigger photon and hadrons that are on the same side of the event, i.e., that have an azimuthal angle ϕ within $\pm90°$ of that of the photon. Such hadrons originate from the bremsstrahlung processes discussed in Sec. II. One of the high-p_T scattered partons radiates a hard photon, and the remainder fragments into hadrons in the usual way. The presence of the accompanying same-side hadrons is thus the signal of the bremsstrahlung component of the production mechanism. This contribution to the photon yield partially obscures the simpler direct-photon contributions from the Compton and annihilation terms that are characterized by the presence of isolated high-p_T photons. In principle, the direct and bremsstrahlung components can be separated by grouping the events into two classes—those with accompanying same-side hadrons and those without. This simple idea is complicated by the fact that in order for a bremsstrahlung photon to have a large transverse momentum, it must take a significant fraction of the parent parton's momentum. This means that the accompanying hadrons will have relatively low transverse momenta and may be difficult to isolate from the beam and target remnants. In addition, the fragmentation process will give the hadrons some transverse momentum with respect to the original parton direction of motion. When this is combined with the relatively small longitudinal momentum fraction possessed by an individual hadron, it becomes likely that, on average, there will be a sizable angular separation between the photon and the associated had-

rons. The photon in a bremsstrahlung event may, therefore, appear to be isolated from the hadrons in the event.

In Fig. 25, results from the AFS Collaboration (Åkesson et al., 1982) are shown for the azimuthal distribution of charged particles relative to γ and π^0 triggers. The large peak at $\phi \approx \pi$ is from the recoiling jet, while the small peak near $\phi \approx 0$ in the π^0 case is from the hadrons associated with the trigger. Notice that the forward peak is essentially absent in the case of a γ trigger. These data have been corrected for the effects of the π^0 decays on the γ distributions.

The dashed lines in Fig. 25 indicate the charged-particle distributions measured in minimum-bias events. If this is interpreted as the charged-particle background from the beam and target jets, the ratio of the bremsstrahlung cross section to the total photon cross section can be measured. The results are shown in Fig. 26 by the solid circles. As a second estimate, the charged-hadron distribution at $\phi = 70°$ was used to estimate the background. The resulting bremsstrahlung ratio is shown in Fig. 26 by the open circles. The predictions from both the Set 1 and the Set 2 distributions are also shown in Fig. 26. Although the errors are large, the data are consistent with the theoretical prediction of a modest bremsstrahlung contribution that decreases with increasing transverse momentum. The theoretical curves suggest that the fall-off with p_T is rather slow, and that one must be prepared to deal with a bremsstrahlung "background" until rather large p_T values. Another point worth mentioning is that,
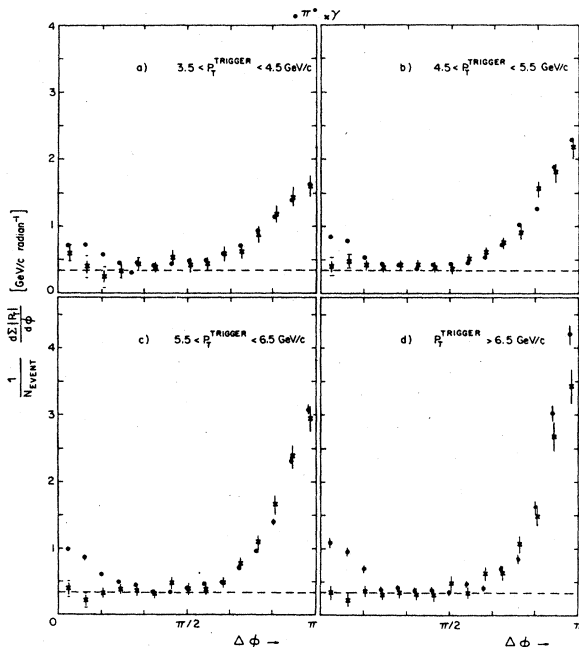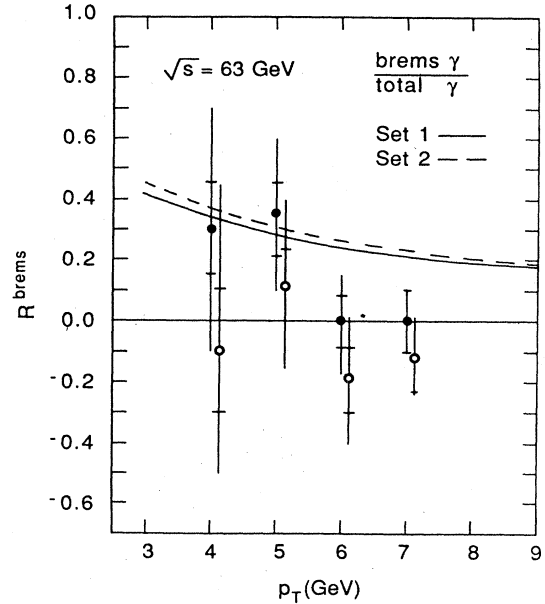

FIG. 26. Experimental estimates of the ratio of the bremsstrahlung contribution and the total photon rate from Åkesson et al. (1982) compared with the theoretical estimates discussed in the text. The two data sets correspond to different methods of performing the subtraction of the background due to the beam and target fragments.

up to logarithmic scaling violation corrections, the bremsstrahlung total ratio is basically a function of x_T. Therefore one must be prepared to accept rather significant bremsstrahlung contributions at the energies and transverse momenta encountered in typical $\bar{p}p$ collider experiments. For example, the bremsstrahlung/total ratio is shown versus x_T for several values of $\sqrt{s}$ in Fig. 27. Clearly the effect is significant.
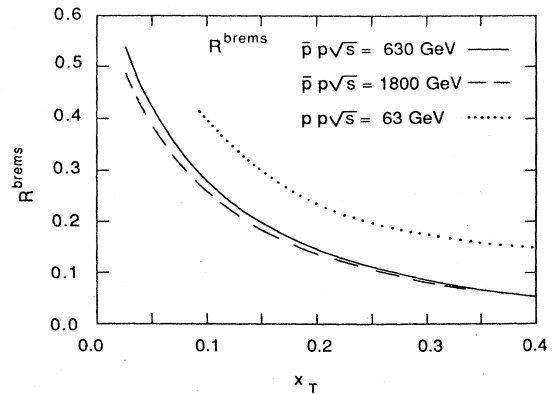

FIG. 25. Azimuthal distributions of the summed p_T of charged hadrons for different bins of γ or π^0 trigger momentum. The γ data have been corrected for the effects of meson-induced background. The data are from Åkesson et al. (1982).

FIG. 27. Theoretical predictions for R^{brems} at various center-of-mass energies shown vs x_T.

2. Away-side hadrons

Consider next the correlations between the trigger photon and hadrons that are on the opposite side of the event, i.e., those having an azimuthal angle ϕ relative to the photon that is larger than $\pm 90°$. If the hadrons have sufficiently large transverse momentum, then they can be interpreted as having resulted from the fragmentation of the recoiling parton. In the case of the Compton process this will be a quark, whereas for the annihilation contribution it will be a gluon. Since the photon couples to electric charge, the expectation for the Compton process is that the recoiling quark will most likely be a u quark. In proton-proton collisions the ratio of u to d quarks on the away side will be approximately 8, with a factor of 4 coming from the square of the quark charge and a factor of 2 from the fact that there are two valence u quarks and one valence d quark in the proton. This 8-to-1 ratio at the quark level gives rise to an expectation of a large ratio of positive to negative hadrons on the away side. This expectation must be modified somewhat since u quarks can give rise to negative hadrons, and d quarks can yield positive hadrons. Nevertheless, there should be a substantially larger fraction of positive hadrons in direct-photon production than in high-p_T events with a hadron trigger. Furthermore, for a fixed value of the trigger p_T, this fraction should increase with the away-side p_T; this follows because the average value of z in the fragmentation process increases, and this increases the correlation between the charge of the hadron and the charge of the fragmenting quark. Calculations of this away-side charge ratio are shown in Fig. 28 together with data from (Åkesson et al. (1982). The expected rise with away-side p_T is consistent with the data, although the errors are sufficiently large that a definite conclusion cannot be drawn. For comparison, results are also shown for events with a π^0 trigger. Again, the errors are large, but the predictions seem to

conform to the trends of the data. For additional discussions of away-side correlations see Baier, Engels, and Petersson (1980) and Benary, Gotsman, and Lissauer (1983).

At this time, extensive correlation studies are available only for proton-proton interactions. However, second-generation experiments using other beams will be able to explore such correlations in greater detail. For example, by taking appropriate combinations of beam types it should be possible to isolate a sample of events dominated by the annihilation process. For this sample the away-side charge ratio should be approximately 1, since the fragmenting parton would be a gluon.

3. Measuring parton distribution and fragmentation functions

The possibility exists to go beyond simple away-side charge ratios and actually measure fragmentation and distribution functions. In order to do this, one must be able to reconstruct the away-side jet, and thereby constrain the parton scattering kinematics. An interesting example that serves to illustrate the potential of such measurements is provided by some recent preliminary results from the AFS Collaboration, which were presented at the 1985 European Physical Society Conference at Bari. A discussion of the results may be found in the review talk on large-momentum-transfer processes by Treille (1985). In Fig. 29 data are shown for the p_T distribution for events in which the photon and recoiling jet both have pseudorapidities near zero. In the absence of a bremsstrahlung contribution, with its extra degree of freedom coming from the fragmentation process, the leading-logarithm predictions for this observable would require no integrations. The momentum fractions of the colliding partons would both be just x_T. The situation is quite analogous to that for the di-jet cross section discussed earlier. However, here there are only two subprocesses, provided that one can neglect the bremsstrahlung component. The data shown in Fig. 29 have been subjected to a photon isolation cut in an attempt to suppress the bremsstrahlung contribution. The effectiveness of this cut is difficult to assess, however. The solid and dashed curves in Fig. 29 show the Set 1 predictions with and without the bremsstrahlung contribution. The Q^2 definition was chosen to be $p_T^2/2$. Clearly, both curves are somewhat flatter than the data. if the final data show this same effect, then this may be an indication that a softer gluon distribution is needed.

It is worth recalling that the di-jet data in Figs. 7—9 were well described by the same formalism that yields the predictions shown in Fig. 29. If a softer gluon distribution is needed to describe the direct-photon data, then some other alterations will be needed to restore good agreement with the di-jet data. Of course, there is still the flexibility of changing the Q^2 definition so as to alter the overall normalization when using the leading-logarithm approximation. An interesting analysis would be to study simultaneously both the di-jet and the photon-jet cross
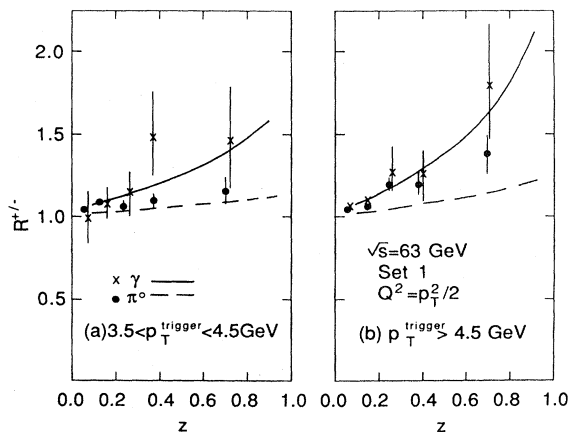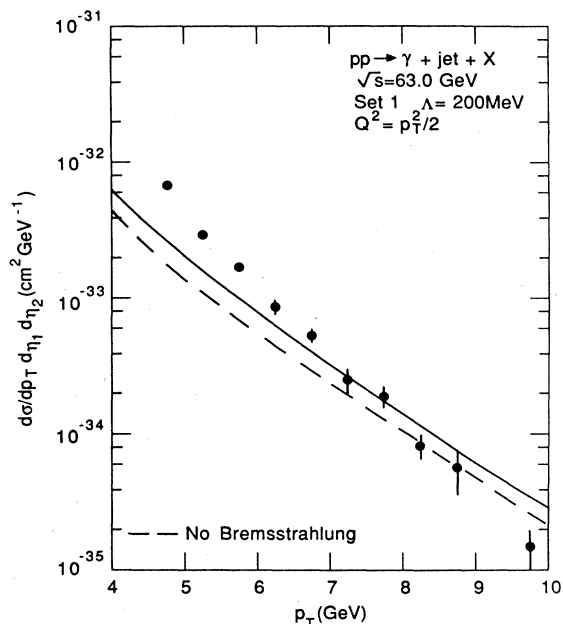

FIG. 28. Comparison between theoretical predictions and experimental data from Åkesson et al. (1982) for the ratio of positive to negative hadrons opposite a neutral trigger. The γ data have been corrected for the effects of the meson-induced background.

FIG. 29. Comparison between the theoretical predictions discussed in the text and data for γ-jet p_T distribution from the AFS Collaboration (Åkesson et al., 1985).
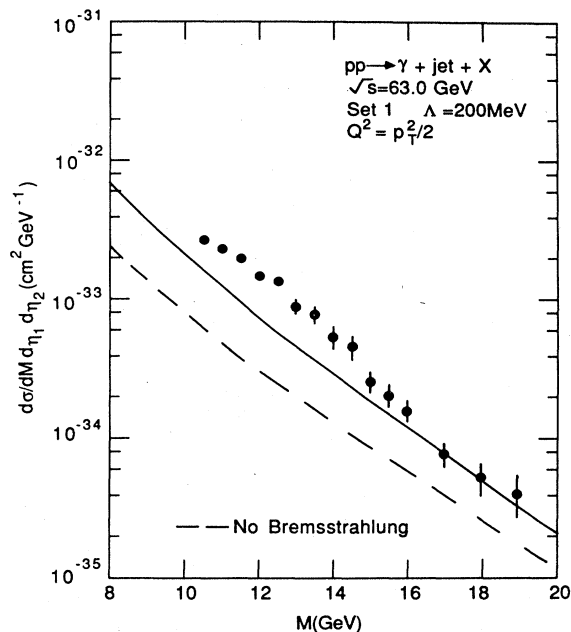
FIG. 30. Comparison between the theoretical predictions discussed in the text and data for γ-jet mass distribution from the AFS Collaboration (Åkesson et al., 1985).

sections in the next-to-leading-logarithm approximation.

The photon-plus-jet data from the AFS Collaboration have also been presented as a function of the photon-jet invariant mass. At the level of two-body subprocesses, this is just the parton-parton center-of-mass energy $\sqrt{\hat{s}}$. If only the Compton and annihilation contributions were present, then the mass and p_T distributions would be simply related because $M = 2p_T$ at $\eta_1 = \eta_2 = 0$. Specifically, at $p_T = M/2$

$$\frac{d\sigma}{d\eta_1 d\eta_2 dp_T} = 2\frac{d\sigma}{d\eta_1 d\eta_2 dM} \; .$$

However, the data for the two distributions are nearly equal, with the mass distribution being somewhat larger in the middle region. This may indicate a substantial bremsstrahlung component, as can be seen by comparing the solid curves in Figs. 29 and 30. The addition of the bremsstrahlung component brings the two distributions into near equality, since the effect is relatively larger for the mass distribution than for the p_T distribution. In the bremsstrahlung case the transverse momentum of the photon is reduced by a factor of z from that of the parent parton. Therefore the bremsstrahlung contribution at a fixed value of photon p_T actually originates from a scattering configuration in which the parent parton had p_T/z. The steep p_T dependence of the cross section means that the bremsstrahlung contribution is suppressed relative to that of the Compton and annihilation subprocesses. This is the usual suppression due to the extra fragmentation. On the other hand, the photon-jet invari-

ant mass is reduced only by a factor of $\sqrt{z}$, so that the suppression is less and the bremsstrahlung contribution is relatively more important. An additional possibility is that the jet identification algorithm results in a photon-jet mass that does not satisfy $M = 2p_T$, where p_T is the transverse momentum of the photon. This would alter the simple relation between the two distributions. Such questions will have to be resolved in order to exploit fully the potential of observables such as these.

Two papers have recently appeared in which the photon-jet correlation data are discussed. In the paper of Argyres, Contogouris, Mebarki, and Vlassopulos (1986), results similar to those shown in Figs. 29 and 30 are presented. In addition, several other parton distributions are used in order to compare with the data. The best comparison is found with the CDHS distributions, which are very similar to Set 1, except that the gluon is somewhat softer. A separate analysis has been published by Aurenche, Baier, Fontannaz, and Schiff (1986a). They point out that, in the two-scale optimized predictions, the running coupling always has an argument smaller than the factorization scale. Even though a complete next-to-leading-order calculation has not been performed for the photon-jet cross section, they argue that this may be true for the optimized correlation calculation as well. If this is true, then the cross-section predictions will be increased, especially at the lower end of the p_T scale. They show that the Set 1 distributions yield a result in substantial agreement with the data. Clearly there is room for more progress in this area on both the theoretical and the experimental sides.

4. Measuring parton-parton scattering angular distributions

Recently, the UA-1 (Arnison et al., 1984) and UA-2 (Bagnaia et al., 1984) Collaborations have presented results on the angular distributions of parton-parton scattering averaged over all of the contributing subprocesses. As shown by Eq. (A10), the two-jet cross section can be written as a differential cross section with respect to $\cos\theta^*$, where θ^* is the parton-parton center-of-mass scattering angle. Experimentally, a boost is performed from the laboratory frame to the di-jet rest frame, and θ^* is then determined for the event as the angle between the di-jet axis and the hadron-hadron axis. This assumes that the initial-state hadrons are collinear in this frame, which will be the case as long as the transverse momenta of the two jets are equal. The theoretical expression involves no integrations, since the measurement of the four-vectors of each jet completely determines the kinematics, provided that parton k_T effects are negligible. The result is a weighted average of the quark-quark, quark-gluon, and gluon-gluon scattering angular distributions. The data from both groups are shown in Fig. 31, together with the predictions from the Set 1 distributions with $Q^2=p_T^2$, shown by the solid curve. The agreement is quite good. It is interesting to note that the role of the scaling violations in the parton distributions and the variation of the running coupling are essential for obtaining the good agreement shown. To see this, note that increasing $\cos\theta^*$ results in a decrease in p_T for fixed di-jet mass. With x_a

and x_b fixed, decreasing p_T results in a relative increase of the parton distributions. In addition, the running coupling also increases. The net result is a relatively steeper angular distribution, since the distribution is normalized to unity at $\cos\theta^*=0$. For comparison, the choice $Q^2=\hat{s}/4$ results in the dashed curve. With this choice, there is no scaling violation or change in the running coupling as $\cos\theta^*$ is varied at fixed di-jet mass. The results are correspondingly less steep in $\cos\theta^*$.

A similar analysis was presented by the CCOR Collaboration (Angelis et al., 1982), in which leading π^0's were used in place of jets. This complicates the theoretical interpretation somewhat, but a reasonably compact result can be derived as shown by Eq. (A11). A selection of the data is shown in Fig. 32, together with the Set 1 predictions obtained with $Q^2=p_T^2$ (solid curves) and $Q^2=\hat{s}/4$ (dashed curves). The same trend is present as for the di-jet case. It is interesting to note that the distributions obtained with the di-pion trigger are somewhat steeper than those obtained with the di-jet trigger. This is due in part to the factor of p_{Tj}^{-1}, which appears in Eq. (A11) and results from the Jacobian used to transform from the parton variables to those defined by the CCOR group.

The same type of measurements as shown in Figs. 31 and 32 can be performed using γ-jet or γ-hadron final states. The γ-jet measurements would be the most straightforward to interpret since, in the absence of the
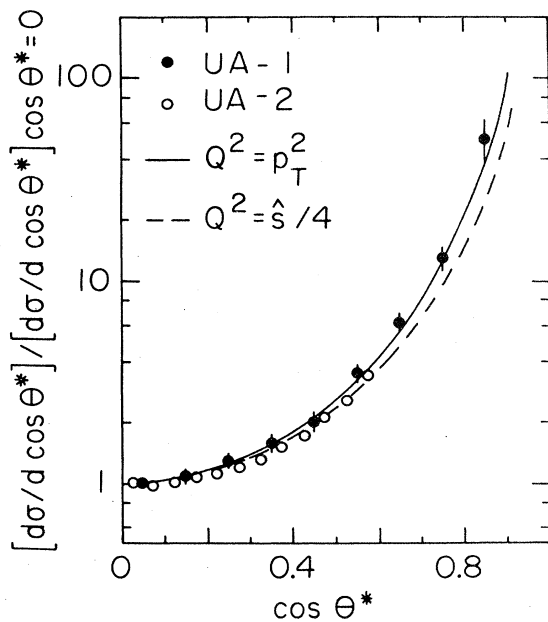

FIG. 31. Comparison between the leading-logarithm predictions discussed in the text and data for the subprocess averaged parton-parton angular distribution: ●, as measured by the UA-1 Collaboration (Arnison et al., 1984); ○, as measured by the UA-2 Collaboration (Bagnaia et al., 1984).
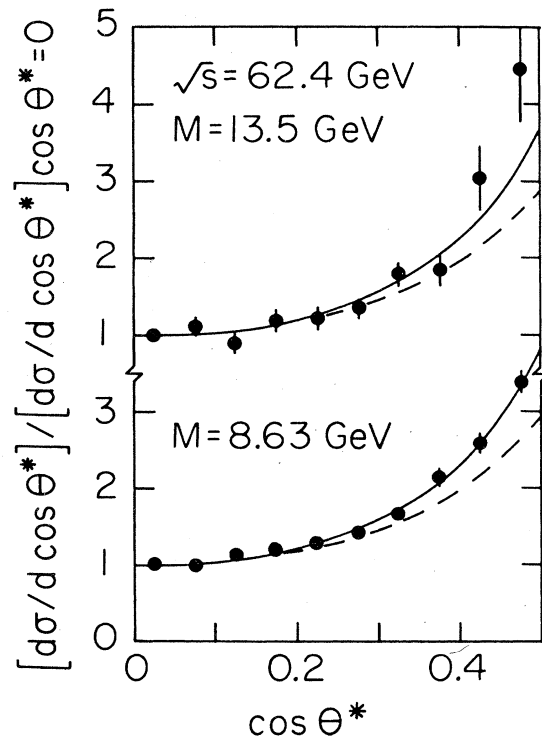

FIG. 32. Comparison between the leading-logarithm predictions discussed in the text and data for the subprocess averaged parton-parton angular distribution as measured by the CCOR Collaboration using a $\pi^0\pi^0$ trigger (Angelis et al., 1982).

bremsstrahlung component, this case would be just like that for the di-jets. However, especially for fixed-target experiments, it may be difficult to identify and reconstruct the recoil jet. In that case, it might be better to utilize the leading away-side hadron as an indicator of the jet direction. The scattering angle could be estimated by boosting to the frame in which the photon and the recoiling hadron were back-to-back. Such a measurement would be of great interest because of the strikingly different angular distribution expected for the Compton subprocess. The dominant two-body parton-parton scattering subprocesses have either t- and/or u-channel poles (e.g., $qq \rightarrow qq$) or a sum of s-, t-, and u-channel poles (e.g., $gg \rightarrow gg$, $gq \rightarrow gq$). The angular distributions are sharply peaked in the forward and backward directions ($\cos\theta^* = \pm 1$). If the angular dependence is parametrized as

$$\frac{d\sigma}{d\cos\theta^*} = \frac{1}{2} \left[\frac{1}{(1+\cos\theta^*)^n} + \frac{1}{(1-\cos\theta^*)^n} \right]$$

and the exponent n is determined by fitting over the range $|\cos\theta^*| \leq 0.5$, then for $gg \rightarrow gg$, $gq \rightarrow gq$, and $qq \rightarrow qq$ one finds $n = 2.02$, 2.15, and 2.6, respectively. Notice that the gluon subprocesses are flatter, reflecting the presence of the s-channel pole term. The corresponding value of n for the Compton subprocess is $n = 0.9$. The much flatter behavior is due to the fact that the Compton subprocess has an s-channel and a u-channel pole term, but no t-channel term, as can be seen in Fig. 2(a). This is illustrated in Fig. 33, which shows predictions for the angular distribution from proton-proton scattering, with a leading positively charged particle opposite the photon. The same cuts as those employed by the CCOR Collaboration were used. The solid curve shows the full result, whereas the dashed curve shows the result of suppressing the bremsstrahlung contribution. For comparison the dotted curve shows the prediction for a $\pi^0\pi^0$ trigger. The difference appears to be large enough to be measurable.

Thus far, all of the photon-hadron correlations have been discussed in the framework of the independent fragmentation model. However, it is also possible to formulate a model based on the fragmentation of strings, as in the Lund model (Andersson, Gustafson, and Sjöstrand, 1980). There are specific effects predicted in the Lund approach that are discussed in Andersson, Bengston, and Gustafson (1982). The observation of these effects requires the ability to detect the away-side hadrons. The forthcoming second-generation experiments will be able to make such measurements.

Although the preceding discussion does not exhaust the possibilities opened up by the advent of correlation data involving direct photons, I believe it does serve to suggest the potential usefulness of such data.

D. Two-photon hadroproduction

The production of two high-p_T photons in hadronic collisions is a process of considerable theoretical interest.
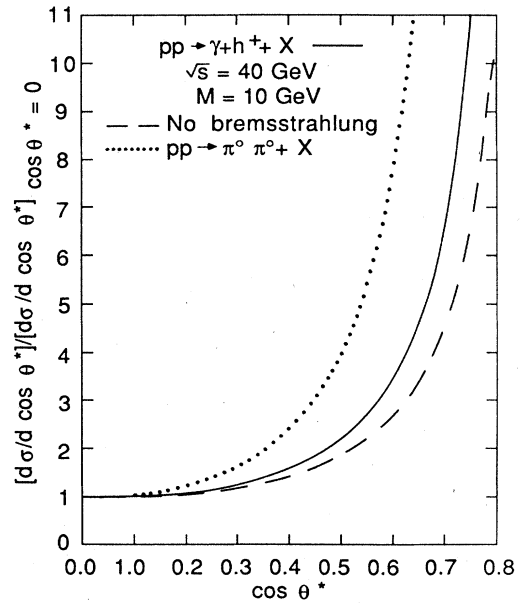

FIG. 33. Angular dependence predicted for a photon-hadron measurement in pp interactions at $\sqrt{s} = 40$ GeV with a positive hadron on the away side. The same cuts as were used for the CCOR determination have been used here. The solid curve shows the full result, while the dashed curve results from suppressing the bremsstrahlung contribution. The dotted curve shows the corresponding result for a $\pi^0\pi^0$ trigger.

The simplest subprocess for this reaction is just QED annihilation, $q\bar{q} \rightarrow \gamma\gamma$, as shown in Fig. 34(a). If parton transverse momenta are neglected, the two photons will be on opposite sides of the event with balancing transverse momenta. The resulting cross section is proportional to the fourth power of the charge of the participating quark. Therefore, if only this subprocess were present, it would be possible to measure the average value of the fourth power of the quark charges by comparing the rate with that for single photons produced by the subprocess $q\bar{q} \rightarrow \gamma g$. This latter cross section can be isolated by taking the cross-section difference between π^- and π^+ or
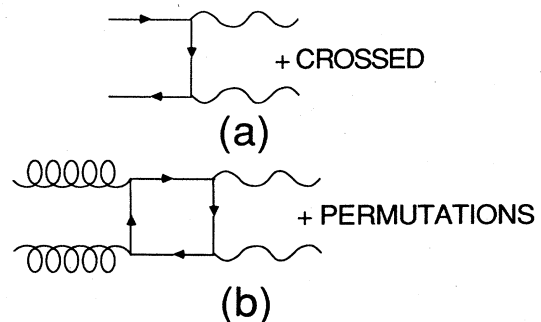

FIG. 34. Two-photon-hadroproduction subprocesses: (a) $q\bar{q} \rightarrow \gamma\gamma$; (b) $gg \rightarrow \gamma\gamma$.

proton and antiproton beams, for example. However, the actual situation is much more complex due to the presence of several other sources of photon pairs. One is the subprocess illustrated in Fig. 34(b), $gg \rightarrow \gamma\gamma$. The gluon distribution is comparable to or larger than the quark distributions at low x values. Therefore, this subprocess can make a significant contribution to the photon yield at low values of x_T. This has been discussed by Combridge (1980) and Carimalo, Crozon, Kessler, and Parisi (1981).

Another important source of photon pairs is direct-photon production from $q\bar{q} \rightarrow \gamma g$ and $gq \rightarrow \gamma q$, with the second photon originating from bremsstrahlung from the recoiling parton. This contribution can be comparable to or larger than that of the two Born term subprocesses. In addition, there will be a contribution from the usual two-body parton-parton subprocesses, in which both recoiling partons give rise to bremsstrahlung photons.

As a result of these various additional sources of photon pairs, the production process is not as simple to interpret as it might appear to be at first sight. However, each of the contributions can be calculated, so that tests based on this reaction are still possible, as is discussed in the paper of Contogouris, Marleau, and Pire (1982). A detailed review of two-photon hadroproduction, treated in the leading-logarithm approximation, can be found in Berger, Braaten, and Field (1984). Indeed, even the next-to-leading-logarithm corrections have been calculated (Aurenche, Douiri, Baier, Fontannaz, and Schiff, 1985).

Recently, three experimental groups have obtained results on the cross section for the production of photon pairs. The results of the AFS Collaboration (Åkesson et al., 1986) are shown in Fig. 35, along with earlier results from Kourkoumelis et al. (1982). A charged multiplicity cut was used in isolating the candidate events, and consequently the bremsstrahlung contribution should be reduced to some extent. However, as has been discussed previously, this reduction is difficult to calculate accurately if leading-logarithm kinematics are used. The prediction from just the $q\bar{q}$ and gg subprocesses of Fig. 34 is shown by the dashed curve, while the solid curve has the bremsstrahlung contributions included. Notice that the latter terms increase the cross section by up to a factor of 3. The Set 1 distributions were used for these curves with $Q^2 = p_T^2/2$. The slight turnover at the low-p_T end is due to a cut that required that each photon have $p_T \geq 1.1$ GeV. Within the rather large errors, the comparison between theory and experiment appears to be reasonable except, perhaps, at the lowest point. However, it should be noted that possible backgrounds from massive states decaying into two photons have not been taken into account. This may account for the discrepancy in the low-mass region.

The NA-3 Collaboration has also obtained results on the photon pair cross section from proton, π^-, and π^+ beams at a beam energy of 200 GeV (Badier et al., 1985). The data are in the region of transverse momentum below 3 GeV, and are, therefore, in a region where perturbation theory may not be applicable. The cross sections have been compared with theoretical predictions obtained using
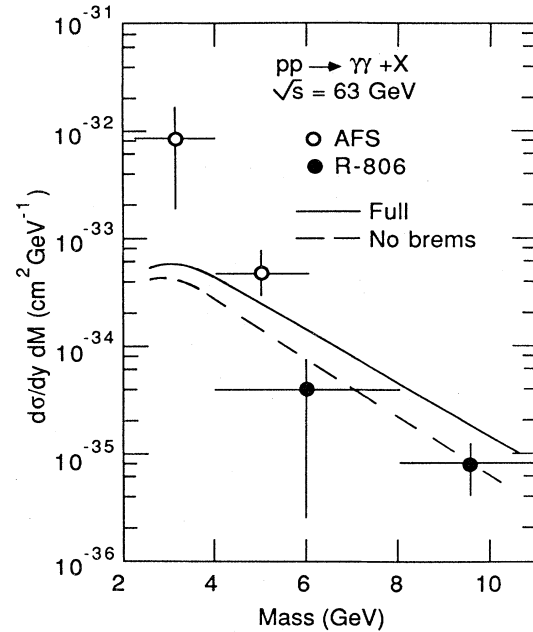

FIG. 35. Comparison between the theoretical predictions discussed in the text and data for two-photon hadroproduction: O, from Åkesson et al. (1986b); ●, from Kourkoumelis et al. (1982). The R-806 data has been plotted as in Åkesson et al. (1986b).

the program of Aurenche, Douiri, Baier, Fontannaz, and Schiff (1985). The π^- data are about a factor of 6 above the predictions, and the corresponding factor for the proton data is about 30. There is, however, a tendency for these ratios to decrease with increasing transverse momentum. In addition, the experimental errors are still large. Clearly, additional high statistics data will be needed at a variety of energies before any detailed conclusions can be drawn.

IV. SUMMARY AND CONCLUSIONS

The study of large-momentum-transfer hadron-hadron scattering has contributed substantially to our understanding of the nature of short-distance parton-parton interactions. Especially with the advent of the high-energy $p\bar{p}$ colliders, such interactions have been successfully described by utilizing the well-known techniques of perturbation theory. We are now at a point where the sophistication of direct-photon experiments is yielding data that can be combined with jet and hadron data to provide new and exciting information on the underlying parton distribution and fragmentation functions and the parton-parton scattering processes themselves.

In this review I have tried to emphasize each of the major ingredients that goes into the calculation of a typical hard-scattering process. The range of possible theoretical predictions depends on the assumptions and approximations utilized. Special attention was devoted to the imprecision that is inherent in the use of the leading-logarithm

approximation. We are now in the fortunate position of having available all of the basic ingredients needed for the calculation of the next-to-leading-logarithm corrections for various observables. Some of these calculations have already been completed, mostly for the single-particle invariant cross section. The new data becoming available for more complicated observables, such as the di-jet or photon-jet cross sections, provide a real challenge for theorists to complete the required higher-order calculations.

The single dominant conclusion that I wish to stress is that there is broad agreement between the data and the theory in all the cases examined here—jets, hadrons, and photons. The data appear to support the theoretical expectations for the energy dependence, event structure, and even normalization, although the uncertainties, particularly on the last quantity, are large. This certainly provides strong encouragement to tackle the additional calculations necessary in order to further refine the comparison with the data.

ACKNOWLEDGMENTS

APPENDIX

The purpose of this appendix is to provide a compact summary of the theoretical expressions used in calculating the various observables discussed in this review. This summary will presumably be of benefit to persons newly introduced to this subject and will also serve to delineate the limitations of the formalism used.

By now a reasonably standard notation has evolved for describing large-transverse-momentum phenomena. For the sake of completeness, however, the notation used in the review is summarized first. Upper-case letters will be used to designate hadrons, in either the initial or the final state, such as $A + B \rightarrow C + X$, etc. Lower-case letters will be used when referring to the hadron constituents that are undergoing the hard scatters.

When discussing the kinematics for single-particle inclusive reactions it is useful to use the Mandelstam variables. If A and B are the initial-state hadrons and C is the observed final-state hadron with four-vectors p_A, p_B, and p_C, respectively, then the Mandelstam variables are defined as

$$s = (p_A + p_B)^2, \quad t = (p_A - p_C)^2 ,$$

and

$$u = (p_B - p_C)^2 .$$

The variable s is simply the square of the center-of-mass energy, while t and u are the squares of the four-momentum transfers from particles A and B to particle C. A similar set of variables exists for the constituent scattering subprocess $a + b \rightarrow c + d$, and a "caret" symbol will be placed over the variable in this case. For the case of massless two-body scattering the Mandelstam variables satisfy the constraint $\hat{s} + \hat{t} + \hat{u} = 0$.

A number of additional variables will be encountered in discussions of large-transverse-momentum processes. These include momentum components that are transverse or longitudinal with respect to the beam direction. These are denoted by p_T and p_l, respectively. Occasionally reference will be made to their scaled counterparts $x_T = 2p_T/\sqrt{s}$ and $x_F = 2p_l/\sqrt{s}$. With these definitions the allowed ranges of x_T and x_F are $(0,1)$ and $(-1,1)$, respectively, if the masses of the hadrons are neglected. Another variable that is often used is the rapidity y, which is defined as

$$y = \tfrac{1}{2} \ln \frac{E + p_l}{E - p_l} .$$

This expression, when evaluated for a massless particle, has a much simpler form. Then, $y = \ln \cot \theta/2$, where θ is the center-of-mass scattering angle. This latter form is convenient experimentally, since one needs to know only θ. For a massive particle the quantity $\ln \cot \theta/2$ is called the pseudorapidity, usually denoted by η. Note that for many high-energy processes the dependence on the particle masses is negligible and that, therefore, the rapidity and pseudorapidity become equivalent.

In the derivations that follow, it will often be necessary to work directly with the four-vectors of the interacting partons. Suppose that parton a carries a fraction x_a of hadron A's longitudinal momentum and that a similar definition for x_b exists for parton b. Then in the overall hadron-hadron center-of-mass system the four-vectors for a and b can, assuming massless partons and neglecting any parton transverse momenta, be written as

$$p_a = \frac{x_a \sqrt{s}}{2}(1,0,0,1) \quad \text{and} \quad p_b = \frac{x_b \sqrt{s}}{2}(1,0,0,-1) ,$$

where the positive z axis is taken to be along the direction of the incident hadron A. If the scattered parton c has transverse momentum p_T and rapidity y_1, then its four-vector is just

$$p_c = p_T(\cosh y_1, 1, 0, \sinh y_1) .$$

With these results it is easy to evaluate the Mandelstam variables at the parton level:

$$\hat{s} = x_a x_b s, \quad \hat{t} = -x_a p_T \sqrt{s}\, e^{-y_1} ,$$

and

$$\hat{u} = -x_b p_T \sqrt{s}\, e^{y_1} .$$

For the case of two-body scattering, the parton Mandelstam variables can also be written in terms of the four-vector of the recoiling parton d, in the event that correlations are being studied. Let

$$p_d = p_T(\cosh y_2, -1, 0, \sinh y_2) \ .$$

Then, $\hat{t}$ and $\hat{u}$ may also be written as

$$\hat{t} = -x_b p_T \sqrt{s}\ e^{y_2} \quad \text{and} \quad \hat{u} = -x_a p_T \sqrt{s}\ e^{-y_2} \ .$$

The following expressions have all been obtained using

massless collinear kinematics. The discussion in Sec. II.E should be sufficient to enable one to generalize these results to the case in which parton k_T effects are included. However, this usually requires the use of Monte Carlo techniques, due to the resulting large number of integrations. For reasons of compactness, the various Q^2 dependences will not be explicitly shown in the following equations.

Starting with two-body scattering at the parton level, the partial cross section for the inclusive production of two partons can be written as

$$d\sigma(AB \to cd) = \frac{1}{2\hat{s}} \sum_{ab} G_{a/A}(x_a)dx_a G_{b/B}(x_b)dx_b \sum |M(ab \to cd)|^2 (2\pi)^4 \delta^4(p_a + p_b - p_c - p_d) \frac{d^3 p_c}{(2\pi)^3 2E_c} \frac{d^3 p_d}{(2\pi)^3 2E_d} \ .$$

$$\text{(A1)}$$

There are implied spin and color sum/averages in the above expression. At the level of two-body scattering, one associates a jet with each of the outgoing partons. However, when more complicated final states are taken into account, e.g., $2 \to 3$ processes, the jet must be carefully defined using energy and angular size cuts, for example.

In order to convert Eq. (A1) into the invariant cross section for inclusive single-jet production, it is easiest to use

$$\frac{d^3 p_d}{2E_d} = d^4 p_d \delta(p_d^2)$$

to integrate over p_d using the four-dimensional δ function. In addition, with massless partons $\delta(p_d^2)$ may be replaced by $\delta(\hat{s} + \hat{t} + \hat{u})$. This results in

$$E \frac{d^3 \sigma}{d^3 p}(AB \to \text{jet} + X) = \sum_{abcd} \int dx_a dx_b G_{a/A}(x_a) G_{b/B}(x_b) \frac{\hat{s}}{\pi} \frac{d\sigma}{d\hat{t}}(ab \to cd) \delta(\hat{s} + \hat{t} + \hat{u}) \ , \tag{A2}$$

where the differential cross section for the two-body parton scattering subprocesses is denoted by

$$\frac{d\sigma}{d\hat{t}}(ab \to cd) = \frac{1}{16\pi \hat{s}^2} \sum |M(ab \to cd)|^2 \ .$$

The argument of the δ function in Eq. (A2) can be expressed in terms of x_a and x_b using the results given above. The x_b integration may then be done with the final result

$$E \frac{d^3 \sigma}{d^3 p}(AB \to \text{jet} + X) = \sum_{abcd} \int_{x_{a\min}}^1 dx_a G_{a/A}(x_a) G_{b/B}(x_b) \frac{2}{\pi} \frac{x_a x_b}{2x_a - x_T e^y} \frac{d\sigma}{d\hat{t}}(ab \to cd) \ , \tag{A3}$$

where $x_b = (x_a x_T e^{-y})/(2x_a - x_T e^y)$ and $x_{a\min} = (x_T e^y)/(2 - x_T e^{-y})$. Equation (A3) is also applicable for the calculation of the direct-photon inclusive invariant cross section resulting from the subprocesses $q\bar{q} \to \gamma g$ and $gq \to \gamma q$.

Next, in order to calculate the single-particle inclusive invariant cross section, the fragmentation function $D_{h/c}(z_c)$ must be included. This function, when multiplied by dz_c, gives the probability for obtaining a hadron h from parton c with the hadron carrying a fraction z_c of the parton's momentum. Using $d^3 p/E = z_c^2 d^3 p_c/E_c$, we find that the resulting expression is

$$E \frac{d^3 \sigma}{d^3 p}(AB \to h + X) = \sum_{abcd} \int dx_a dx_b dz_c G_{a/A}(x_a) G_{b/B}(x_b) D_{h/c}(z_c) \frac{\hat{s}}{\pi z_c^2} \frac{d\sigma}{d\hat{t}}(ab \to cd) \delta(\hat{s} + \hat{t} + \hat{u}) \ . \tag{A4}$$

As in the previous case, the argument of the δ function may be expressed in terms of the parton kinematic variables, and the z_c integration may then be done. The final form for the cross section is

$$E \frac{d^3 \sigma}{d^3 p}(AB \to h + X) = \sum_{abcd} \int_{x_{a\min}}^1 dx_a \int_{x_{b\min}}^1 dx_b G_{a/A}(x_a) G_{b/B}(x_b) D_{h/c}(z_c) \frac{1}{\pi z_c} \frac{d\sigma}{d\hat{t}}(ab \to cd) \ , \tag{A5}$$

where

$$z_c = \frac{x_T}{2x_b} e^{-y} + \frac{x_T}{2x_a} e^y, \quad x_{b\min} = \frac{x_a x_T e^{-y}}{2x_a - x_T e^y}, \quad \text{and} \quad x_{a\min} = \frac{x_T e^y}{2 - x_T e^{-y}} \ .$$

Equation (A5) is also applicable for the calculation of the single-photon inclusive invariant cross section when the photon results from the fragmentation from one of the scattered partons. In this case one must replace $D_{h/c}$ with $D_{\gamma/c}$.

The above equations for the invariant cross sections include a summation over all of the possible two-body parton scattering subprocesses. The expressions for these are given in Table I. In addition, the summation implies a symmetrization under $\hat{t}$ and $\hat{u}$ interchange, i.e., interchanging the beam and target. Note that for the case of three quark flavors there are 127 terms contributing to the inclusive single-particle cross section.

The partial cross section in Eq. (A1) can also be used as the basis for calculating a two-jet inclusive cross section. In the absence of parton k_T effects, the transverse-momentum components of the δ function ensure that the jets are produced with equal and opposite transverse momenta. The di-jet cross section can then be written in terms of the rapidities of the two jets and the transverse momentum p_T possessed by each:

$$\frac{d\sigma}{dy_1 dy_2 dp_T^2}(AB \rightarrow \text{jet}_1 + \text{jet}_2 + X) = \sum_{ab} \int dx_a dx_b G_{a/A}(x_a) G_{b/B}(x_b)$$

$$\times \frac{\hat{s}}{2} \frac{d\sigma}{d\hat{t}}(ab \rightarrow 12) \delta \left[x_a \frac{\sqrt{s}}{2} + x_b \frac{\sqrt{s}}{2} - p_T \cosh y_1 - p_T \cosh y_2 \right]$$

$$\times \delta \left[x_a \frac{\sqrt{s}}{2} - x_b \frac{\sqrt{s}}{2} - p_T \sinh y_1 - p_T \sinh y_2 \right] . \tag{A6}$$

The two δ functions appearing in Eq. (A6) are the energy and longitudinal parts of the original four-dimensional δ function appearing in Eq. (A1). Together, they allow the integrations on both x_a and x_b to be carried out. The resulting two-jet cross section is

$$\frac{d\sigma}{dy_1 dy_2 dp_T^2}(AB \rightarrow \text{jet}_1 + \text{jet}_2 + X) = \sum_{ab} x_a G_{a/A}(x_a) x_b G_{b/B}(x_b) \frac{d\sigma}{d\hat{t}}(ab \rightarrow 12) , \tag{A7}$$

where

$$x_a = \frac{p_T}{\sqrt{s}}(e^{y_1} + e^{y_2}) \quad \text{and} \quad x_b = \frac{p_T}{\sqrt{s}}(e^{-y_1} + e^{-y_2}) .$$

Another variable that is often used in studies of jet production is the di-jet invariant mass M_{jj}^2. This is easily shown to be given by

$$M_{jj}^2 = 2p_T^2[1 + \cosh(y_1 - y_2)] , \tag{A8}$$

if the masses of the individual jets are neglected. The mass distribution is given by

$$\frac{d\sigma}{dy_1 dy_2 dM_{jj}} = \frac{M_{jj}}{1 + \cosh(y_1 - y_2)} \frac{d\sigma}{dy_1 dy_2 dp_T^2} . \tag{A9}$$

Equation (A9) has been used to calculate the curves shown in Fig. 7.

The di-jet cross section in Eq. (A7) has no integrations remaining to be performed. That is, knowledge of the four-vectors of the two jets has completely determined the kinematics of the parton scattering process. Thus it is possible to use Eq. (A7), or an equivalent expression, to determine the parton-parton scattering angular distribution, averaged over all of the participating subprocesses. Let θ^* be the parton-parton center-of-mass scattering angle. Then, Eq. (A7) can be rewritten as

$$\frac{d\sigma}{dx_a dx_b d\cos\theta^*} = \frac{x_a x_b s}{2} \sum_{ab} G_{a/A}(x_a) G_{b/B}(x_b) \frac{d\sigma}{d\hat{t}}(ab \rightarrow 12) , \tag{A10}$$

where x_a and x_b have the same values as for Eq. (A7).

It is also possible to perform similar measurements with the two jets replaced by high-p_T hadrons. In this case the expressions are somewhat more complicated by the fact that the hadrons represent fragments of the jets. It is useful to define several additional variables. Let M and Y be the invariant mass and rapidity of the dihadron system, respectively. Furthermore, let Δ denote the difference between the two hadron transverse momenta. That is, Δ is the transverse momentum of the dihadron system. In general, Δ is a two-dimensional transverse vector. However, for the simplified kinematics being considered here, Δ and the transverse momenta of the two hadrons will all lie in the same plane. In addition, let M_{jj} and Y_{jj} denote the invariant mass and rapidity of the di-jet system, respectively. In the event that parton k_T effects are neglected, it is straightforward to derive the following relations:

$$M^2 = z_1 z_2 M_{jj}^2, \quad \Delta = p_{Tj}(z_1 - z_2) \, ,$$

$$Y_{jj} = Y + \ln\frac{M_T}{M} - \ln\left[\left[\frac{z_1}{z_2}\right]^{1/2} \frac{1+\cos\theta^*}{2} + \left[\frac{z_2}{z_1}\right]^{1/2} \frac{1-\cos\theta^*}{2} \right] \quad \text{with } M_T = \sqrt{M^2 + \Delta^2} \, .$$

Here p_{Tj} is the transverse momentum of the jet that fragments into the observed hadron. With the simplified kinematics resulting from the neglect of parton k_T effects, the two jets have balancing transverse momenta, and p_{Tj} is given by

$$p_{Tj}^2 = \frac{M_{jj}^2}{4}(1 - \cos^2\theta^*) \, .$$

With these results it is possible to construct the following differential cross section:

$$\frac{d\sigma}{dM^2 dY \, d\Delta \, d\cos\theta^*} = \int \frac{d\sigma}{dM_{jj}^2 dY_{jj} d\cos\theta^*} dM_{jj}^2 dY_{jj} dz_1 dz_2$$

$$\times D_{h_1/j_1}(z_1) D_{h_2/j_2}(z_2)\delta(M^2 - z_1 z_2 M_{jj}^2)\delta[\Delta - (z_1 - z_2)p_{Tj}]$$

$$\times \delta\left\{ Y_{jj} - Y - \ln\frac{M_T}{M} + \ln\left[\left[\frac{z_1}{z_2}\right]^{1/2} \frac{1+\cos\theta^*}{2} + \left[\frac{z_2}{z_1}\right]^{1/2} \frac{1-\cos\theta^*}{2} \right] \right\} \, ,$$

where

$$\frac{d\sigma}{dM_{jj}^2 dY_{jj} d\cos\theta^*} = \frac{1}{2}\frac{d\sigma}{dy_1 dy_2 dp_{Tj}^2}$$

from Eq. (A7). The δ functions allow three of the integrations to be performed. The final expression may be written as

$$\frac{d\sigma}{dM^2 dY \, d\Delta \, d\cos\theta^*} = \int dz_1 \frac{d\sigma}{dM_{jj}^2 dY_{jj} d\cos\theta^*} D_{h_1/j_1}(z_1) D_{h_2/j_2}(z_2) \frac{2}{z_1 p_{Tj}(z_1 + z_2)} \, , \tag{A11}$$

with

$$Y_{jj} = Y + \frac{1}{2}\ln\left[1 + \frac{\Delta^2}{M^2} \right] - \ln(r\cos\theta^* + \sqrt{1+r^2}), \quad \sqrt{z_2} = \sqrt{z_1}(-r + \sqrt{1+r^2}), \quad r = \frac{\Delta}{M\sin\theta^*} \, ,$$

$$M_{jj} = \frac{M}{\sqrt{z_1 z_2}}, \quad \text{and} \quad \frac{M}{\sqrt{s}}e^{|Y_{jj}|} \leq \sqrt{z_1} \leq \min(1, r + \sqrt{1+r^2}) \, .$$

The jet cross section in Eq. (A11) is given by

$$\frac{d\sigma}{dM_{jj}^2 dY_{jj} d\cos\theta^*} = \frac{x_a x_b}{2} \sum_{abcd} G_{a/A}(x_a)G_{b/B}(x_b)\frac{d\sigma}{d\hat{t}}(ab \to cd) \, ,$$

with $x_a = (M_{jj}/\sqrt{s})e^{Y_{jj}}$ and $x_b = (M_{jj}/\sqrt{s})e^{-Y_{jj}}$.

This particular form for the dihadron cross section is particularly well suited to the implementation of the cuts used by the CCOR Collaboration (Angelis *et al.*, 1982). As discussed in Sec. III.C.4, symmetric high-p_T trigger experiments are not particularly sensitive to parton k_T-smearing effects and, therefore, Eq. (A11) yields results that are in close agreement with a detailed Monte Carlo calculation in which k_T effects are included.

Parton scattering angular distributions can also be measured in reactions in which one of the arms contains a photon. For the case of a bremsstrahlung photon, Eq. (A11) can be used with the appropriate photon fragmentation function appearing in the integrand. If, however, the photon originates directly from a two-body subprocess such as $qg \to \gamma q$ or $q\bar{q} \to \gamma g$, then the z_1 fragmentation function should be replaced by $\delta(1 - z_1)$, allowing the last integration to be performed.

The formalism discussed above can be used to determine the shapes of the parton-parton scattering angular distributions. In addition, correlations between the trigger photon and the recoiling away-side hadrons in direct-photon events can also yield useful information. In principle it would be best if the entire away-side jet could be reconstructed, so that each hadron could be assigned its respective momentum fraction z. In practice, it is often difficult to uniquely assign soft hadrons to a particular jet, and an alternative method is needed. A useful variable in this instance is x_e, defined as

$$x_e = -\frac{\mathbf{p}_{Th} \cdot \mathbf{p}_{T\gamma}}{p_{T\gamma}^2} \, ,$$

where $\mathbf{p}_{T\gamma}$ and $\mathbf{p}_{Th}$ are the transverse momenta of the trigger photon and the observed away-side hadron, respectively. If

parton k_T effects and hadron masses are neglected, x_e becomes equal to the usual momentum fraction z. If only the subprocesses $gq \rightarrow \gamma q$ and $q\bar{q} \rightarrow \gamma g$ are used, then the x_e distribution can be calculated using

$$\frac{d\sigma}{dy_\gamma dp_{T\gamma}^2 dx_e} = \sum_{abd} \int dx_a dx_b G_{a/A}(x_a) G_{b/B}(x_b) \hat{s} \frac{d\sigma}{d\hat{t}}(ab \rightarrow \gamma d) D_{h/d}(x_e) \delta(\hat{s}+\hat{t}+\hat{u}) \ . \tag{A12}$$

In Eq. (A12) the integration ranges for x_a and x_b are the same as for Eq. (A5). If, on the other hand, bremsstrahlung photons are included in the trigger, then the photon can have less than the full energy of the parent jet. In this case the away-side hadron can actually have a larger transverse momentum than the trigger photon, and x_e can be greater than one. The presence of the photon fragmentation function means that one additional integration must be performed. The resulting expression is

$$\frac{d\sigma}{dy_\gamma dp_{T\gamma}^2 dx_e} = \sum_{abcd} \int_{x_{a\min}}^1 dx_a \int_{x_{b\min}}^1 dx_b G_{a/A}(x_a) G_{b/B}(x_b) \frac{d\sigma}{d\hat{t}}(ab \rightarrow \gamma d) D_{\gamma/c}(z_c) D_{h/d}(z_2) \ , \tag{A13}$$

where

$$z_2 = x_e z_1 \ ,$$

$$z_1 = \frac{x_T}{2x_b} e^{-y_1} + \frac{x_T}{2x_a} e^{y_1} \ ,$$

$$z_{1\max} = \min(1/x_e, 1) \ ,$$

$$x_{b\min} = \frac{x_a x_T e^{-y_1}}{2x_a z_{1\max} - x_T e^{y_1}} \ ,$$

$$x_{a\min} = \frac{x_T e^{y_1}}{2z_{1\max} - x_T e^{-y_1}} \ .$$

REFERENCES

Abramowicz, H., et al., 1982, Z. Phys. C 12, 289.

Abramowicz, H., et al., 1983, Z. Phys. C 17, 283.

Åkesson, T., et al., 1982, Phys. Lett. B 118, 178.

Åkesson, T., et al., 1983, Phys. Lett. B 123, 133.

Åkesson, T., et al., 1984, Z. Phys. C 25, 13.

Åkesson, T., et al., 1985, paper presented at the 1985 European Physical Society Conference in Bari (unpublished); Direct Photon Plus Away-side Jet Production at $\sqrt{s}$ =63 GeV and a Determination of the Gluon Distribution, CERN Report No. CERN-EP 186-195.

Åkesson, T., et al., 1986a, Z. Phys. C 30, 27.

Åkesson, T., et al., 1986b, Z. Phys. C 32, 491.

Altarelli, G., R. K. Ellis, M. Greco, and G. Martinelli, 1984, Nucl. Phys. B 246, 12.

Altarelli, G., and G. Parisi, 1977, Nucl. Phys. B 126, 298.

Althoff, M., et al., 1984, Z. Phys. C 22, 307.

Anassontzis, E., et al., 1982, Z. Phys. C 13, 277.

Anderson, K. J., et al., 1979, Phys. Rev. Lett. 43, 1219.

Andersson, B., H.-U. Bengston, and G. Gustafson, 1982, Event Structure in Reactions with Prompt Photons, University of Lund Report No. LU TP 82-10.

Andersson, B., G. Gustafson, and T. Sjöstrand, 1980, Phys. Lett. B 94, 211.

Angelis, A. L. S., et al., 1980, Phys. Lett. B 94, 106.

Angelis, A. L. S., et al., 1982, Nucl. Phys. B 209, 284.

Appel, J. A., et al., 1985, Phys. Lett. B 160, 349.

Appel, J. A., et al., 1986, Phys. Lett. B 176, 239.

Arenton, M. W., et al., 1985, Phys. Rev. D 31, 984.

Argyres, E. P., A. P. Contogouris, N. Mebarki, and S. D. P. Vlassopulos, 1986, McGill University report, 1986.

Argyres, E. P., A. P. Contogouris, M. Sanielevici, and H. Tanaka, 1984, Phys. Rev. D 29, 2527.

Arnison, G., et al., 1984, Phys. Lett. B 136, 294.

Arnison, G., et al., 1986a, Phys. Lett. B 172, 461.

Arnison, G., et al., 1986b, Nucl. Phys. B 276, 253.

Aurenche, P., R. Baier, M. Fontannaz, and D. Schiff, 1986a, Phys. Lett. B 169, 441.

Aurenche, P., R. Baier, M. Fontannaz, and D. Schiff, 1986b, Dealing with Ambiguities in Higher Order QCD Predictions for Large p_T Processes Involving Real Photons, Orsay Report No. LPTHE 86/14.

Aurenche, P., A. Douiri, R. Baier, M. Fontannaz, and D. Schiff, 1984, Phys. Lett. B 140, 87.

Aurenche, P., A. Douiri, R. Baier, M. Fontannaz, and D. Schiff, 1985, Z. Phys. C 29, 423.

Aurenche, P., and J. Lindfors, 1980, Nucl. Phys. B 168, 296.

Badier, J., et al., 1985, Phys. Lett. B 164, 184.

Badier, J., et al., 1986, Z. Phys. C 31, 341.

Bagger, J., and J. F. Gunion, 1982, Phys. Rev. D 25, 2287.

Bagnaia, P., et al., 1984, Phys. Lett. B 144, 283.

Baier, R., J. Engels, and B. Petersson, 1979, Z. Phys. C 2, 265.

Baier, R., J. Engels, and B. Petersson, 1980, Z. Phys. C 6, 309.

Banner, M., et al., 1985, Z. Phys. C 27, 329.

Bardeen, W. A., 1984, talk presented at the 6th International Workshop on Photon-Photon Collisions, Lake Tahoe, California. Available as FERMILAB-CONF-84/133-T.

Barnett, R. M., and D. Schlatter, 1982, Phys. Lett. B 112, 475.

Benary, O., E. Gotsman, and D. Lissauer, 1981, Z. Phys. C 9, 81.

Benary, O., E. Gotsman, and D. Lissauer, 1983, Z. Phys. C 16, 211.

Berger, E. L., 1980a, Phys. Lett. B 89, 241.

Berger, E. L., 1980b, Z. Phys. C 4, 289.

Berger, E. L., 1982, Phys. Rev. D 26, 105.

Berger, E. L., E. Braaten, and R. D. Field, 1984, Nucl. Phys. B 239, 52.

Berger, E. L., and S. J. Brodsky, 1979, Phys. Rev. Lett. 42, 940.

Berger, E. L., T. Gottschalk, and D. Sivers, 1981, Phys. Rev. D 23, 99.

Blankenbecler, R., S. J. Brodsky, and J. F. Gunion, 1972, Phys. Lett. B 39, 649.

Blankenbecler, R., S. J. Brodsky, and J. F. Gunion, 1973, Phys. Lett. B 42, 461.

Blankenbecler, R., S. J. Brodsky, and J. F. Gunion, 1975, Phys. Rev. D 12, 3469.

Blankenbecler, R., S. J. Brodsky, and J. F. Gunion, 1978, Phys.

Rev. D **18**, 900.

Bloch, F., and A. Nordsieck, 1937, Phys. Rev. **52**, 54.

Breakstone, A., et al., 1984, Phys. Lett. B **135**, 505.

Buras, A. J., 1980, Rev. Mod. Phys. **52**, 199.

Burkert, V., 1983, in *Gluons and Heavy Flavours,* Proceedings of the Hadronic Session of the Eighteenth Rencontre de Moriond, edited by J. Tran Thanh Van (Editions Frontières, Gif-sur-Yvette), Vol. I. p. 189.

Carimalo, C., M. Crozon, P. Kessler, and J. Parisi, 1981, Phys. Lett. B **98**, 105.

Caswell, W. E., R. R. Horgan, and S. J. Brodsky, 1978, Phys. Rev. D **18**, 2415.

Celmaster, W., and D. Sivers, 1982, Ann. Phys. (N.Y.) **143**, 1.

Collins, J. C., D. E. Soper, and G. Sterman, 1985, Nucl. Phys. B **250**, 199.

Combridge, B., 1980, Nucl. Phys. **174**, 243.

Contogouris, A. P., 1982, Phys. Rev. D **26**, 1618.

Contogouris, A. P., R. Gaskell, and L. Marleau, 1980, Phys. Rev. D **22**, 1109.

Contogouris, A. P., L. Marleau, and B. Pire, 1982, Phys. Rev. D **25**, 2459.

Contogouris, A. P., N. Mebarki, and H. Tanaka, 1986, Hard Real Photon Processes at Collider, ISR, and Fixed Target Energies, McGill University report.

Contogouris, A. P., N. Mebarki, H. Tanaka, and S. D. P. Vlassopulos, 1985, Phys. Rev. D **32**, 1134.

Contogouris, A. P., S. Papadopoulos, and M. Hongoh, 1979, Phys. Rev. D **19**, 2607.

Contogouris, A. P., S. Papadopoulos, and C. Papavassiliou, 1981, Nucl. Phys. B **179**, 461.

Contogouris, A. P., S. Papadopoulos, and J. Ralston, 1981, Phys. Lett. B **104**, 70.

Contogouris, A. P., S. Papadopoulos, and J. P. Ralston, 1982, Phys. Rev. D **26**, 1280.

Contogouris, A. P., and H. Tanaka, 1985, Hadron. J. **8**, 1.

Contogouris, A. P., and H. Tanaka, 1986, Phys. Rev. D **33**, 1265.

Cormell, L. R., et al., 1985, Phys. Lett. B **150**, 322.

Cormell, L. R., and J. F. Owens, 1980, Phys. Rev. D **22**, 1609.

Darriulat, P., 1980, Annu. Rev. Nucl. Part. Sci. **30**, 159.

Dechantsreiter, M., F. Halzen, and D. M. Scott, 1981, Phys. Rev. D **24**, 2856.

DeMarzo, C., et al., 1985, in *Proceedings of the XVI International Symposium on Multiparticle Dynamics,* edited by J. Grunhaus (Editions Frontières, Gif-sur-Yvette), p. 149.

Devoto, A., D. W. Duke, J. F. Owens, and R. G. Roberts, 1983, Phys. Rev. D **27**, 508.

DeWitt, R. J., L. M. Jones, J. D. Sullivan, D. E. Williams, and H. D. Wyld, Jr., 1979, Phys. Rev. D **19**, 2046; **20**, 1751(E).

DiLella, L., 1985, Annu. Rev. Nucl. Sci. **35**, 107.

Duke, D. W., and J. F. Owens, 1984, Phys. Rev. D **30**, 49.

Duke, D. W., and R. G. Roberts, 1985, Phys. Rep. **120**, 275.

Ellis, R. K., H. Georgi, M. Machacek, H. D. Politzer, and G. C. Ross, 1978, Phys. Lett. B **78**, 281.

Ellis, R. K., H. Georgi, M. Machacek, H. D. Politzer, and G. C. Ross, 1979, Nucl. Phys. B **152**, 285.

Ellis, J., and C. T. Sachrajda, 1980, in *Quarks and Leptons,* Proceedings of the 1979 Cargèse Summer Institute on Quarks and Leptons, edited by M. Lévy, J.-L. Basdevant, D. Speiser, J. Weyers, R. Gastmans, and M. Jacob (Plenum, New York/London), p. 285.

Ellis, R. K., and J. C. Sexton, 1986, Nucl. Phys. B **269**, 445.

Ellis, S. D., and R. Stroynowski, 1977, Rev. Mod. Phys. **9**, 753.

Escobar, C. O., 1975, Nucl. Phys. B **98**, 173.

Farrar, G., 1977, Phys. Lett. B **67**, 337.

Farrar, G., and G. C. Fox, 1980, Nucl. Phys. B **167**, 205.

Farrar, G., and S. C. Frautschi, 1976, Phys. Rev. Lett. **36**, 1017.

Ferbel, T., 1986, Acta Phys. Pol. B **17**, 435.

Ferbel, T., and W. R. Molzon, 1984, Rev. Mod. Phys. **56**, 181.

Feynman, R. P., R. D. Field and G. C. Fox, 1978, Phys. Rev. D **18**, 3320.

Field, R. D., 1979, in *Quantum Chromodynamics,* AIP Conference Proceedings No. 55, edited by W. Frazer and F. Henyey (American Institute of Physics, New York), p. 97.

Frisch, H. J., et al., 1980, Phys. Rev. Lett. **44**, 511.

Fritzsch, H., M. Gell-Mann, and H. Leutwyler, 1973, Phys. Lett. B **47**, 365.

Fritzsch, M., and P. Minkowski, 1977, Phys. Lett. B **69**, 316.

Glück, M., K. Grassie, and E. Reya, 1984, Phys. Rev. D **30**, 1447.

Gottschalk, T. D., 1986, Nucl. Phys. B **277**, 700.

Gross, D. J., and F. Wilczek, 1973a, Phys. Rev. Lett. **30**, 1343.

Gross, D. J., and F. Wilczek, 1973b, Phys. Rev. D **8**, 3633.

Grunberg, G., 1980, Phys. Lett. B **95**, 70.

Grunberg, G., 1984, Phys. Rev. D **29**, 2315.

Gupta, S., and A. H. Mueller, 1979, Phys. Rev. D **20**, 118.

Halzen, F., and D. M. Scott, 1978a, Phys. Rev. Lett. **40**, 1117.

Halzen, F., and D. M. Scott, 1978b, Phys. Rev. D **18**, 3378.

Halzen, F., and D. M. Scott, 1980a, Phys. Rev. D **21**, 1320.

Halzen, F., and D. M. Scott, 1980b, Phys. Rev. D **22**, 1609.

Horgan, R. R., and P. N. Scharbach, 1981, Nucl. Phys. B **181**, 421.

Jacob, M., and P. V. Landshoff, 1978, Phys. Rep. **48**, 285.

Jones, D., and J. F. Gunion, 1979, Phys. Rev. D **19**, 867.

Kaplan, D. M., et al., 1978, Phys. Rev. Lett. **40**, 435.

Kourkoumelis, C., et al., 1980, Z. Phys. C **5**, 95.

Kourkoumelis, C., et al., 1982, Z. Phys. C **16**, 101.

Lepage, G. P., and S. J. Brodsky, 1980, Phys. Rev. D **22**, 2157.

McCubbin, N. A., 1981, Rep. Prog. Phys. **44**, 1027.

Møller, R., 1984, Acta Phys. Pol. B **15**, 989.

Naudet, C., et al., 1986, Phys. Rev. Lett. **56**, 808.

Owens, J. F., 1978, Phys. Lett. B **76**, 85.

Owens, J. F., 1979, Phys. Rev. D **19**, 3279.

Owens, J. F., 1982a, in *Multiparticle Dynamics 1981,* edited by W. D. Shephard and V. P. Kenney (World Scientific, Singapore), p. 553.

Owens, J. F., 1982b, Surv. High Energy Phys. **3**, 65.

Owens, J. F., 1984, Phys. Rev. D **30**, 943.

Owens, J. F., 1985a, *QCD and Beyond,* Proceedings of the Hadronic Session of the Twentieth Rencontre de Moriond, edited by J. Tran Thanh Van (Editions Frontières, Gif-sur-Yvette), Vol. I, p. 151.

Owens, J. F., 1985b, *Multiparticle Dynamics,* Proceedings of the Twenty-Six Symposium, Kiryat Anavim, Israel, edited by S. Grunhaus (World Scientific, Singapore).

Owens, J. F., and J. D. Kimel, 1978, Phys. Rev. D **18**, 3313.

Palestini, S., et al., 1985, Phys. Rev. Lett. **55**, 2649.

Pennington, M., 1983, Rep. Prog. Phys. **46**, 393.

Politzer, H. D., 1973, Phys. Rev. Lett. **30**, 1346.

Politzer, H. D., 1982, Nucl. Phys. B **194**, 493.

Reya, E., 1981, Phys. Rep. **69**, 195.

Rückl, R., S. J. Brodsky, and J. F. Gunion, 1979, Phys. Rev. D **18**, 2469.

Rutherfoord, J. P., 1985, *Rapporteur's talk at the 1985 International Symposium on Lepton and Photon Interactions at High Energies,* Kyoto, Japan, edited by M. Konuma and K. Takahashi (Kyosho, Japan), p. 662.

Sivers, D., S. J. Brodsky, and R. Blankenbecler, 1976, Phys.

Rep. **23**, 1.

Sjöstrand, T., 1985, Phys. Lett. B **157**, 321.

Soh, K. S., P. Y. Pac, H. W. Lee, and J. B. Choi, 1978, Phys. Rev. D **18**, 751.

Sterman, G., 1986, Phys. Lett. B **179**, 281.

Sterman, G., 1987, Nucl. Phys. B **281**, 310.

Stevenson, P. M., 1981a, Phys. Lett. B **100**, 61.

Stevenson, P. M., 1981b, Phys. Rev. D **23**, 2916.

't Hooft, G., and M. Veltman, 1972, Nucl. Phys. B **144**, 189.

Treille, D., 1985, Hard Scattering of Hadrons and Photons, Rappateur's talk given at the International Conference on High Energy Physics, Bari, CERN Report No. CERN-EP/85-181.

Uematsu, T., 1978, Phys. Lett. B **79**, 97.